HHS Public Access

Author manuscript

Neuroimage. Author manuscript; available in PMC 2017 March 01.

Published in final edited form as:

Neuroimage. 2016 March ; 128: 167–179. doi:10.1016/j.neuroimage.2015.12.026.

Probabilistic maps of the white matter tracts with known associated functions on the neonatal brain atlas: application to evaluate longitudinal developmental trajectories in term-born and preterm-born infants

Kentaro Akazawa[a], **Linda Chang**[b], **Robyn Yamakawa**[b], **Sara Hayama**[b], **Steven Buchthal**[b], **Daniel Alicata**[b], **Tamara Andres**[b], **Deborrah Castillo**[b], **Kumiko Oishi**[c], **Jon Skranes**[d], **Thomas Ernst**[b], and **Kenichi Oishi**[*,a]

[a]Department of Radiology, Johns Hopkins University School of Medicine, Baltimore, MD, USA

[b]Department of Medicine, School of Medicine, University of Hawaii at Manoa, Honolulu, HI, USA

[c]Department of Biomedical Engineering, Johns Hopkins University, Baltimore, MD, USA

[d]Department of Laboratory Medicine, Children's and Women's Health, Norwegian University of Science and Technology, Trondheim, Norway

Abstract

Diffusion tensor imaging (DTI) has been widely used to investigate the development of the neonatal and infant brain, and deviations related to various diseases or medical conditions like preterm birth. In this study, we created a probabilistic map of fiber pathways with known associated functions, on a published neonatal multimodal atlas. The pathways-of-interest include the superficial white matter (SWM) fibers just beneath the specific cytoarchitectonically defined cortical areas, which were difficult to evaluate with existing DTI analysis methods. The Jülich cytoarchitectonic atlas was applied to define cortical areas related to specific brain functions, and the Dynamic Programming (DP) method was applied to delineate the white matter pathways traversing through the SWM. Probabilistic maps were created for pathways related to motor, somatosensory, auditory, visual, and limbic functions, as well as major white matter tracts, such as the corpus callosum, the inferior fronto-occipital fasciculus, and the middle cerebellar peduncle, by delineating these structures in eleven healthy term-born neonates. In order to characterize maturation-related changes in diffusivity measures of these pathways, the probabilistic maps were then applied to DTIs of 49 healthy infants who were longitudinally scanned at three time-points, approximately five weeks apart. First, we investigated the normal developmental pattern based on 19 term-born infants. Next, we analyzed 30 preterm-born infants to identify developmental patterns related to preterm birth. Last, we investigated the difference in diffusion measures

[*]Corresponding author: Kenichi Oishi, M.D., Ph.D., The Russell H. Morgan Department of Radiology and Radiological Science, The Johns Hopkins University School of Medicine, 208 Traylor Building, 720 Rutland Avenue, Baltimore, MD 21205, Work: 410-502-3553, koishi@mri.jhu.edu.

between these groups to evaluate the effects of preterm birth on the development of these functional pathways. Term-born and preterm-born infants both demonstrated a time-dependent decrease in diffusivity, indicating postnatal maturation in these pathways, with laterality seen in the corticospinal tract and the optic radiation. The comparison between term- and preterm-born infants indicated higher diffusivity in the preterm-born infants than in the term-born infants in three of these pathways: the body of the corpus callosum; the left inferior longitudinal fasciculus; and the pathway connecting the left primary/ secondary visual cortices and the motion-sensitive area in the occipitotemporal visual cortex (V5/MT+). Probabilistic maps provided an opportunity to investigate developmental changes of each white matter pathway. Whether alterations in white matter pathways can predict functional outcomes will be further investigated in a follow-up study.

Graphical Abstract

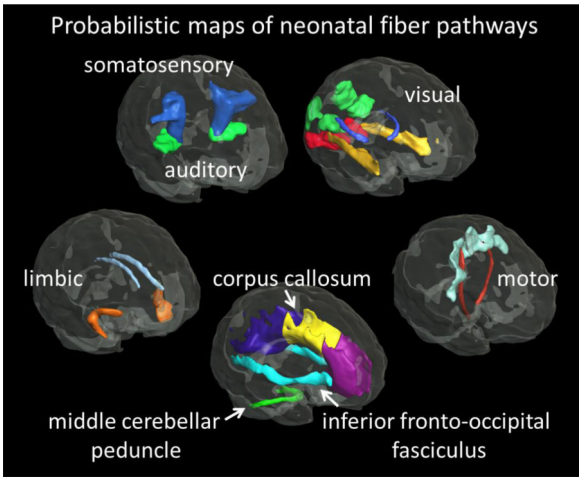

Keywords

Diffusion tensor imaging; Functional pathway; Tractography; Probabilistic map; Neonate; Preterm birth

1. Introduction

Diffusion tensor imaging (DTI) has been widely used to investigate the development of neonatal and infant brains and alterations related to various diseases or medical conditions (Huppi et al., 1998). Whole-brain DTI analysis based on tract-based spatial statistics (TBSS) (Smith et al., 2006), which is suitable for detecting alterations of white matter tracts with high fractional anisotropy (FA), has been applied to evaluate various conditions associated with prematurity at birth: chronic lung disease (Ball et al., 2010); hypoxic-ischemic injury (Gao et al., 2012); hypercapnic ventilation (Ball et al., 2010); small-for-gestational-age infants (Lepomaki et al., 2013); and the neuro-protective effect of erythropoietin therapy for preterm infants (O'Gorman et al., 2015). The major strength of TBSS is the ability to identify highly localized "hot spots" for group differences, without an *a priori* hypothesis. Atlas-based analysis (ABA) is an alternative whole-brain analysis method, in which brain structures are parcellated into more than 100 anatomical structures that cover the entire

brain, and parcel-by-parcel statistical analysis is performed (Oishi et al., 2012). ABA can evaluate the developmental status of individual anatomical units, including gray and white matter structures (Kersbergen et al., 2014; Loh et al., 2012; Oishi et al., 2013; Oishi et al., 2011c; Rose et al., 2014a), and allows the extraction of anatomical features from images that are combined with non-imaging clinical information (Rose et al., 2014b). The tracts-of-interest (TOI) method, in which white matter bundles are defined by tractography and tract-by-tract statistical analysis is performed, is well suited for the evaluation of major white matter bundles that are consistently observed in the human brain (Shi et al., 2014; Taylor et al., 2015). The fiber tracts mapped on images for the TOI are similar to a “roadmap” that visualizes connections between different areas, while parcellation maps from ABA are similar to an “area map” that defines the boundaries of each local region. The TBSS, ABA, and TOI methods are complementary to each other, and altogether, have contributed to the study of the early development of major white matter bundles. Namely, there is a general tendency toward a sharp increase in FA and a decrease in diffusivity measures during the first two years of life, but with variations depending on structures (Mukherjee et al., 2001; Saksena et al., 2008; Trivedi et al., 2009a; Yap et al., 2013; Zhang et al., 2007; Zhang et al., 2005). The limbic fibers are among the most developed structures at birth with the projection (e.g., corticospinal tract or spinothalamic tract) and the commissural (e.g., corpus callosum (CC)) fibers that develop from bottom-to-top and central-to-peripheral directions (Dubois et al., 2006; Gilmore et al., 2007; Huang et al., 2006; Huppi et al., 1998; Yap et al., 2013). The association fibers are the last to mature (Dubois et al., 2008; Huang et al., 2006; Zhang et al., 2007). This observation in DTI measures is congruent with patterns of myelination and axonal growth during early development (Kinney et al., 1988). The FA and diffusivity measures indicated a posterior-to-anterior direction of maturation within white matter regions (Oishi et al., 2011c; Rose et al., 2014a), although there is some controversy about the CC (Braga et al., 2015). Posterior portions of the CC and the projection fibers become detectable in deterministic tractography after their anterior counterparts (Huang et al., 2006). Among DTI measures, the FA increase is affected by tract organization (alignment, direction, and fiber-crossing), and the reduction in diffusion is sensitive to myelination, water content, and macromolecular concentration during early development (Gilmore et al., 2007; Mukherjee et al., 2002; Oishi et al., 2011c).

However, little is known about the development of the superficially located white matter (SWM) fibers (Oishi et al., 2011b; Oishi et al., 2008; Reveley et al., 2015). Investigation of the SWM of the neonatal brain is challenging because there is minimal myelination in neonatal and infant brains, which may lead to very low FA values. Since FA is too low, TBSS, or the conventional TOI methods that target high-FA white matter tracts, are unable to investigate these fibers. Moreover, delineating fibers passing through fiber-crossing areas such as the SWM is difficult with existing deterministic tractography, which relies on the first eigenvector of the tensor. ABA can be used to investigate the SWM (Oishi et al., 2008) although existing neonatal atlases (Brown et al., 2014; Kuklisova-Murgasova et al., 2011; Oishi et al., 2011c; Serag et al., 2012; Shi et al., 2014) do not include specialized parcellation maps for the investigation of the SWM. Since these SWM fibers connect between specific functional cortical regions, measuring the developmental trajectories of the

SWM may provide early indicators that reflect developmental milestones, or predict functional outcomes.

In this study, we investigated white matter pathways known to be associated with various functions including the motor, somatosensory, visual, auditory, and limbic systems, which travel through the SWM areas, and other major white matter fiber tracts, based on our hypothesis that the developmental status of these pathways is related to corresponding functional developments. As an initial step, we created probabilistic maps of neonatal functional pathways on the published neonatal multimodal atlas (Oishi et al., 2011c) to quantify DTI–derived measures of these pathways. These functions include motor, somatosensory, auditory, visual, and limbic systems, the status of which is important as these are the developmental milestones of early life (http://www.nlm.nih.gov/medlineplus/infantandnewborndevelopment.html). The pathways inevitably include SWM fibers just beneath the specific cytoarchitectonically defined cortical areas, which have been difficult to evaluate with existing analysis methods. The two major challenges were: to define cytoarchitectonically defined cortical areas that are usually invisible on conventional MRI or DTI; and to delineate fibers that course through the SWM. We applied the Jülich cytoarchitectonic atlas (Eickhoff, et al., 2005) to define cortical areas related to specific brain functions, and the Dynamic Programming (DP) method (Li et al., 2014; Ratnanather et al., 2013) to delineate the white matter pathways that course through the SWM. DP enables delineation of fibers within fiber-crossing areas using a probabilistic framework. Twenty-six white matter tracts that were categorized into one of the functional pathways (motor, somatosensory, auditory, visual, and limbic pathways), or major white matter bundles, such as the fronto-occipital fasciculus, the CC, and the middle cerebellar peduncle, were delineated on DTIs of 11 normal-term neonates, and normalized to the neonatal atlas. These tracts were binarized and then averaged to create probabilistic maps in the atlas space. To investigate maturation-related diffusion characteristics, the probabilistic maps were applied to DTIs of term- and preterm-born infants, who were longitudinally scanned at three time-points, at approximately five-week intervals, when the brain has the most rapid growth (Holland et al., 2014). We investigated the developmental patterns of term-born and preterm-born infants, and the effects of preterm birth on the developmental pattern.

2. Methods

2.1 Creation of probabilistic maps

2.1.1 Neonates—Eleven de-identified DTIs of term-born neonates (four boys and seven girls born at 38 to 41 postmenstrual weeks, and scanned within three days of life) were used to create the probabilistic atlases. The neonates were born at the Johns Hopkins Hospital. For the database creation, approval was obtained from the Johns Hopkins Medicine Institutional Review Board and the neonates' parents provided written, informed consent. These eleven DTIs were used only for the creation of the probabilistic maps, and not used for the application study described in 2.2.

2.1.2 MRI scans—Scans were performed without sedation on sleeping neonates. Images were acquired using a 3.0 T Philips scanner equipped with gradients of up to 8.0 G/cm per

direction. The radio frequency (RF) was transmitted through a body coil and the receive coil was an eight-element sensitivity encoding (SENSE) coil, in which two of the coils were combined to be connected to a six-channel receiver. Single-shot echo planar imaging (EPI) with SENSE acquisition was used for DTI (Bammer et al., 2001; Jaermann et al., 2004; Pruessmann et al., 1999). The imaging matrix was 80 × 80 with a field-of-view of 150 × 150 mm, which gave a nominal 1.88 mm isotropic in-plane resolution. These were zero-filled to 256 × 256 mm. The slice orientation was axial with a 1.9 mm thickness parallel to the anterior–posterior commissure line. Forty to fifty slices covered the entire brain. Echo time was 71 ms and repetition time was approximately 4670 ms (4670.49 – 4671.14) depending on the number of slices. A SENSE reduction factor of three was used. Diffusion-weighting was applied along 30 separate axes (Jones et al., 1999) with b = 700 s/mm^2 , in addition to five minimally diffusion-weighted images. Scanning time for one complete DTI dataset was approximately five minutes.

2.1.3 Image processing—The raw diffusion-weighted images were first co-registered to one of the minimally diffusion-weighted images using a linear transformation of Automated Image Registration (AIR) (Woods et al., 1998). The six elements of the diffusion tensor were calculated for each pixel with multivariate linear fitting using DtiStudio (H. Jiang and S. Mori, Johns Hopkins University, Kennedy Krieger Institute, lbam.med.jhmi.edu or www.MriStudio.org) (Jiang et al., 2006; Mori et al., 2008; Pierpaoli et al., 2001). After diagonalization, three eigenvalues and eigenvectors were obtained.

2.1.4 Cytoarchitectonic mapping on the JHU-neonate atlas—To date, the only publicly available cytoarchitectonic atlas based on histological examination is the Jülich cytoarchitectonic map (http://www.fz-juelich.de/inm/inm-1/EN/Forschung/_docs/SPMAnatomyToolbox/SPMAnatomyToolbox_node.html) (Eickhoff, et al., 2005), which is overlaid on the adult T1-weighted Colin-27 brain (Holmes et al., 1998). We transformed this cytoarchitectonic map onto the JHU-neonate atlas (Oishi et al., 2011c) to identify cortical areas related to various brain functions. The transformation matrix was obtained by transforming the cortical parcellation map on the Colin-27 brain, “automated anatomical labeling (AAL)” (Tzourio-Mazoyer, et al., 2002), to the parcellation map of the JHU-neonate atlas, using large deformation diffeomorphic metric mapping (LDDMM). Parcellation maps, rather than the T1-weighted images, were chosen to drive the transformation because the image contrast of T1-weighted images of the neonatal brain is substantially different from that of the adult T1-weighted images, and does not provide adequate contrast for anatomical delineations. Specifically, white matter has a higher intensity than the cortex on adult T1-weighted images, while the cortex is more intense than unmyelinated white matter on neonatal T1-weighted images. Cortical gyri defined on the AAL and the JHU-neonate atlases were co-registered through the LDDMM transformation.

2.1.5 Cytoarchitectonic mapping on each neonatal DTI—The JHU-neonate DTI atlas was transformed to each of the 11 brain DTIs using dual-channel LDDMM (Ceritoglu et al., 2009; Oishi et al., 2009). The reported transformation accuracy of this method, measured by the Dice coefficient, were > 0.8 in the deep gray matter structures (Oishi et al., 2011c) and > 0.6 in the cortical area (Zhang et al., 2014). Resultant transformation matrices

were applied to the cytoarchitectonic maps on the JHU-neonate atlas to create cytoarchitectonic maps for each of the 11 neonatal DTIs. Cytoarchitectonic labels used for this study were: the supplementary and premotor cortices (Area 6) (Geyer, 2004); the primary motor cortex (Areas 4a and 4p) (Geyer et al., 1996); the sensory thalamus; the primary somatosensory cortex (Areas 1, 2, 3a, and 3b) (Geyer et al., 1999; Geyer et al., 2000; Grefkes et al., 2001); the primary auditory cortex (Areas TE1.0, 1.1, and 1.2) (Morosan et al., 2001); and the visual cortices (V1, V2, V4, and V5/MT+) (Amunts et al., 2000; Malikovic et al., 2007; Wilms et al., 2005). The medial geniculate body (MGB) was adopted from the JHU-neonate atlas (http://lbam.med.jhmi.edu/), which was manually delineated based on the T1-weighted contrast. The inter-rater reproducibilities of two MGB areas, drawn by two raters, and measured by the Dice coefficient, were 0.837 (left) and 0.877 (right).

2.1.6 Tractography—The functional pathways were depicted using DTI tractography. The names of the pathways studied are listed with the corresponding regions of interest (ROIs) in Table 1. Deterministic tractography (Mori et al., 1999) was applied to construct pathways, using an established tract-tracing protocol (Kaur, et al., 2014; Yamamoto, et al., 2007) that included: the genu, body, and the splenium of the CC; the cingulate fasciculus; the corticospinal tract; the inferior fronto-occipital fasciculus; the inferior longitudinal fasciculus (ILF); the optic radiation; the middle cerebellar peduncle; and the uncinate fasciculus. Briefly, ROIs were drawn manually as described here. The corticospinal tract: the first ROI was placed on the cerebral peduncle in the axial view and the second ROI was placed on the precentral gyrus in the axial view. The optic radiation: the first ROI was placed on the occipital lobe in a coronal view and the second ROI was placed on the lateral geniculate body in a sagittal view. The uncinate fasciculus: the first ROI was placed on the temporal lobe in the coronal view and the second ROI was placed on the inferior part of the frontal lobe in the coronal view. The cingulum bundle: the first ROI was placed on the cingulate gyrus region at the level of the splenium of the CC in the coronal view and the second ROI was placed on the cingulum at the level of the genu of the CC in the coronal view. The ILF: the first ROI covered the entire hemisphere at the level of the posterior edge of the cingulum in the coronal view and the second ROI was placed on the temporal lobe in the coronal view. The inferior fronto-occipital fasciculus: the first ROI was placed on the occipital lobe in the coronal view and the second ROI was placed on the frontal lobe in the coronal view. The middle cerebellar peduncle: the two ROIs were placed on both sides of the middle cerebellar peduncle in the same axial slice. The CC: the ROI was placed on the entire CC at the midsagittal plane.

To depict pathways that pass through SWM areas and connect adjacent cortical areas, or through regions in which multiple white matter bundles cross, we applied the path-finding approach based on the DP (Khaneja et al., 1998; Ratnanather et al., 2003), as detailed previously (Li et al., 2014). This method computes the optimal path (in this study, the functional pathways) linking two regions-of-interest, based on probabilities of the transitions between each voxel on the path and its 26 neighbor voxels. Optimization was achieved by DP, which calculates the path with the lowest cumulative cost of all points on the path. We applied this technique to create known neuronal connections between two anatomical

structures, such as the pathway between the premotor and primary motor cortices, the pathway between the sensory thalamus and the primary somatosensory cortex, the acoustic radiation that connects the MGB and the primary auditory cortex, the pathway that connects the V1/V2 and the V4, and the pathway that connects the V1/V2 and the V5/MT+ (V1/V2 - V5/MT+).

2.1.7 Probabilistic maps of the functional pathways—The pathways constructed by tractography were binarized (inside =1; outside =0) and transformed to the JHU-neonate atlas space, by applying LDDMM matrices derived from transforming individual DTIs to the JHU-neonate atlas. The probabilistic maps were calculated as average images of normalized individual neuronal pathways.

2.2 Application of the probabilistic maps to DTI of term- and preterm-born infants

We applied the probabilistic maps to a set of longitudinally scanned brain DTIs of infants to measure the diffusivity of each neural pathway. The two purposes of the application studies were to characterize the developmental pattern of the white matter pathways in term- and preterm-born infants, and to investigate the effect of preterm birth on developmental patterns.

2.2.1 Participants—Eighty-four term- and preterm-born infants were enrolled. The infants' parents or legal guardians first provided written and verbal informed consent for the study, which was approved by the Co-operative Institutional Review Board of the Queen's Medical Center, the University of Hawaii, and the Johns Hopkins University. Nineteen term-born and 30 preterm-born infants completed the longitudinal study and were clinically evaluated by a physician to ensure they fulfilled the study criteria. Maternal exclusion criteria were: 1) Maternal age<18 years; 2) Inability to fully understand English, which would have precluded informed consent. Exclusion criteria for the term-born infants included: 1) Prolonged intensive care (>7 days); 2) Intracranial hemorrhage; 3) Neonatal encephalopathy; 4) Known Toxoplasmosis, Other (syphilis, varicellazoster, parvovirus B19), Rubella, Cytomegalovirus (CMV), and Herpes (TORCH) infections; 5) Congenital anomaly. Preterm-born infants were excluded if they 1) required supplementary oxygen or mechanical ventilation during the time of scanning; 2) had a circulation, respiratory or airway abnormality; 3) were diagnosed with fever, epilepsy, or active infection. These infants also were evaluated with a modified Amiel-Tison Neurological Assessment for newborns, and all had usable MR scans at three time points, approximately five weeks apart within the first term-equivalent four months of age (Table 2). The motor and somatosensory functions measured by the Amiel-Tison Neurological Assessment, the existence of retinopathy of prematurity (ROP), and the results of the hearing test are included in Table 2 as basic information.

2.2.2 Image acquisition and processing—The infants were scanned without sedation. A vacuum immobilization mat (Noras MRI Products, Hoechberg, Germany) was used to minimize infant motion and earmuffs were used to protect the infants' ears from scanner noise. Images were acquired using a 3.0 T Siemens TIM Trio scanner (Siemens Medical Solutions, Erlangen, Germany) equipped with a 12-channel phased-array RF coil for parallel

imaging. A single-shot EPI acquisition with SENSE was used for DTI. The imaging matrix was 80 × 80 with a field-of-view of 160 × 160 mm, which resulted in a 2 mm isotropic in-plane resolution. The slice orientation was axial, with a 2.5 mm thickness. Forty to fifty slices covered the entire brain. Echo time was 106 ms and repetition time was 7 to 9 sec, depending on specific absorption rate limitations. Diffusion-weighting was applied along 12 independent axes with b = 1000 s/mm^2, in addition to a minimally diffusion-weighted image. After tensor calculation using DtiStudio, each DTI was transformed to the JHU-neonate DTI atlas using dual-channel LDDMM (Oishi et al., 2011c). The trace map (sum of three eigenvalues of the tensor) was calculated from each tensor field that was transformed to the atlas space.

To evaluate brain abnormalities visible on conventional T1- and T2-weighted images, three-dimensional magnetization-prepared rapid gradient-echo (MPRAGE) and three-dimensional Sampling Perfection with Application optimized Contrast using different flip angle Evolutions (SPACE) sequences were acquired with the following parameters. MPRAGE: echo time 4.15 ms, repetition time 3.2 s, flip angle 7°, imaging matrix of 176 × 256 × 160, and a 1 mm isotropic resolution. SPACE: echo time 386 ms, repetition time 3.2 s, imaging matrix of 120 × 204 × 256, and a 1 mm isotropic resolution. These anatomical images were read by a neuroradiologist. No incidental findings were reported.

2.2.3 Data analysis—The trace value was chosen as a parameter to assess the neurodevelopmental status. Reduction in the trace value typically represents a decrease in water content and an increase in membrane density during the first stage of myelination, which leads to a decrease in all eigenvalues of the tensor (Baumann and Pham-Dinh, 2001; Dubois et al., 2008; Neil et al., 2002; Prayer et al., 2001; Wimberger et al., 1995), which correlates well with the developmental status of the white matter (Oishi et al., 2011c). Interpretation of other DTI-derived measures, such as axial and radial diffusivity or anisotropy, is not straightforward in SWM areas since fibers with different orientations in a voxel cause interactions between radial and axial diffusivities and may lead to fictitious changes (Wheeler-Kingshott and Cercignani, 2009). The average trace values of brain regions with a probability of more than 75% was measured for each infant at each time point using the probabilistic maps overlaid on the trace maps and transformed to the atlas space. As the FA value and other diffusivity measures are useful for cross-study comparison, these results were also reported (see Table 1 – 5 in (Chang et al., submitted)).

2.2.3.1 Development of term-born and preterm-born infants: The term- and preterm-born infants were analyzed separately. For each pathway, a mixed model analysis for repeated measures was performed to characterize chronological changes in the trace value related to brain development over three time points, and to investigate the differences in trace values between boys and girls, and the left and right sides of the pathways. The subjects' age, based on postmenstrual weeks at the time of the scans, was used as a covariate to adjust for variation at each time point. A p-value of 0.05, corrected for multiple comparisons (Bonferroni), was used as the threshold.

2.2.3.2 Effect of preterm birth: The term- and preterm-born infants were analyzed together. For each pathway, a mixed model analysis for repeated measures was performed to

characterize chronological changes in the trace values related to brain development over three time points, and to investigate the differences between term- and preterm-born groups. A p-value of 0.05, corrected for multiple comparisons (Bonferroni), was used as the threshold. For the white matter pathways with significant differences between term- and preterm-born groups, a pairwise comparison between groups was performed at each time point to see the difference in the trace values corrected for postmenstrual weeks at scan (corrected trace). The corrected trace values were correlated with the gestational ages at birth to investigate the influence of prematurity on the trace value. A p-value of 0.05, corrected for multiple comparisons (Bonferroni), was used as the threshold. SPSS Statistics 22 (IBM, Armonk, NY) was used for the statistical analyses.

3. Results

3.1 The probabilistic maps of functional pathways

The probabilistic maps of five functional pathways and three major white matter tracts were overlaid on the JHU-neonate atlas for visualization (Fig. 1).

3.2 Application of the probabilistic maps to evaluate developmental changes in diffusion measures

3.2.1 Developmental trajectory of white matter pathways in term-born infants—None of the infants had a brain abnormality visible on conventional T1- and T2-weighted images. The trace value decreased longitudinally in a time-dependent manner, indicating postnatal maturation (Fig. 2). Laterality of the trace value was identified only on the corticospinal tract (left<right, $p=7.41\times10^{-14}$), the optic radiation (left<right, p=0.004), and the pathway connecting the sensory thalamus and the primary somatosensory area (left>right, p=0.008) (Table 3A). The diffusion measures between boys and girls were not different.

3.2.2 Developmental trajectory of white matter pathways in preterm-born infants—None of the infants had brain abnormality visible in conventional T1- and T2-weighted images. The trace value decreased longitudinally in a time-dependent manner as seen in term-born infants (Fig. 2). Laterality of the trace value was identified only on the corticospinal tract (left<right, $p=6.75\times10^{-18}$), the inferior fronto-occipital fasciculus (left<right, p=0.002), and the optic radiation (left<right, p=0.011) (Table 3B). The diffusion measures between boys and girls were not different.

3.2.3 Effect of preterm-birth on developmental trajectories of white matter pathways—Interaction between group status (term versus preterm) and time point was not significant in any of the white matter pathways. The effect of time point on corrected trace values (corrected for the postmenstrual weeks at scan) was significant in most of the white matter pathways (Bonferroni corrected-p<0.05), except for the body of the CC (p = 0.73), the bilateral corticospinal tract (left, p = 0.29; right, p = 0.27), and the right acoustic radiation (p = 0.09). A significant group effect on corrected trace values was identified in the body of the CC (p = 0.009), the left ILF (p = 0.010), and the left V1/V2 – V5/MT+ (p = 0.031) (Table 4). Pairwise comparisons showed significant group effects at all three time

points, with trace values consistently higher in preterm than term-born infants. The trace values for these three pathways, corrected for postmenstrual ages at scan, were negatively correlated with gestational age at birth. This was true for each time-point, with the exception of the left V1/V2 – V5/MT+, which was no longer significant at the third time-point, indicating normalization of the initially elevated trace (Fig. 3). However, relative to the term-born infants, several preterm-born infants with ROP showed persistently elevated trace values in the body of the CC (2/5 with ROP); the left ILF (5/10 with ROP); and in the left V1/V2 – V5/MT+ (2/4 with ROP). The results of other parameters, FA, and the first, second, and third eigenvalues, and the radial diffusivity, are shown in the Tables 1 – 5 of (Chang et al., submitted). Briefly, an age-dependent increase in FA and a decrease in diffusivity measures (eigenvalues and radial diffusivity) were seen in all pathways, and group differences between the term- and preterm-born infants were seen in the body of the CC (1st and 3rd eigenvalues and radial diffusivity), the genu of the CC (3rd eigenvalue), left V1/2 – V4 (1st eigenvalue), the left V1/V2 – V5/MT+ (2nd eigenvalue and radial diffusivity), the right thalamus – primary somatosensory cortex (1st eigenvalue), and the left ILF (2nd and 3rd eigenvalues and radial diffusivity).

4. Discussion

We developed probabilistic maps of white matter tracts with known neuronal functions and evaluated the longitudinal microstructural development in both term- and preterm-born infants within the first four months of term-equivalent age. Despite the relatively normal neurological assessments without visible abnormalities on conventional T1- and T2-weighted images, the preterm-born infants showed less maturity, with higher diffusivity, than the term-born infants in three of these pathways: the CC; the left ILF; and the left primary visual cortex – V5/MT+ area. These findings demonstrate that evaluation of functional pathways using this approach may be more sensitive for assessing regional brain development in early life and for detecting delayed brain development.

4.1 Probabilistic maps of the functional pathways

The fibers passing through the SWM areas connecting cytoarchitectonically defined areas with known functions and other brain structures have been identified. These fibers connect the premotor and primary motor cortices, the thalamus and the primary somatosensory cortex, the medial geniculate body and the primary auditory cortex, and the primary visual and higher visual association cortices. These fiber trajectories were investigated in non-human primates using histology and neuroimaging approaches (Ratnanather et al., 2013; Schmahmann and Pandya, 2006) and compared to brain diffusion MRI results in humans (Berman et al., 2013; Oishi et al., 2011b). The fiber trajectories delineated in this study matched these findings, and we additionally proposed a three-dimensional trajectory between the primary and higher visual association cortices, which was not established previously.

DTI is a promising and sensitive method with which to detect subtle anatomical abnormalities in the neonatal brain (Miller et al., 2007; Mourmans et al., 2006; Neil et al., 2002; Nijman et al., 2013; Oishi et al., 2013; Okumura et al., 2008; Padilla et al., 2014;

Panigrahy and Bluml, 2007; Paquette et al., 2013; Parmar et al., 2004; Pogribna et al., 2013; Porter et al., 2010). To further explore the full potential of DTI, a systematic and quantitative assessment of brain abnormalities is essential to enable an evaluation of the anatomical-functional correlation for better diagnosis and prognosis of various types of anatomical abnormalities. We expect that the proposed probabilistic maps will be suitable to quantify the developmental status of the white matter pathways related to neuronal functions.

A potential future application of the probabilistic maps is the quantification of non-DTI modalities. Since the probabilistic maps are in the multimodal neonatal atlas space, one can transform T1- or T2-weighted images to the corresponding atlas. If quantitative images coregistered to T1- or T2-weighted images are available, the resultant transformation matrix can be applied to transform the quantitative images to the atlas space. For example, from a multiple echo spin echo sequence, a quantitative T2-map as well as a T2-weighted image could be extracted. One can assume the myelination status of each functional pathway by transforming the T2-map to atlas space (Pannek et al., 2013), and by overlaying the probabilistic maps for quantification of T2 values (Oishi et al., 2011a). This approach is especially useful when DTI is not available.

4.2 Development of functional pathways in term- and preterm-born infants

Consistent with previous DTI studies (Dubois et al., 2008; Gao et al., 2009; Provenzale et al., 2007), the longitudinal analyses of the functional pathways and the major white matter tracts in our term- and preterm-born infants indicate a basic pattern in the maturation process, such as a decrease in diffusivity and an increase in anisotropy with age (see Tables 1 – 5 of (Chang et al., submitted)). The decrease in trace values has been interpreted as a result of reduced water content, myelination, and development of cell membranes associated with axons, dendrites, and glial processes (Miller et al., 2002; Mukherjee et al., 2002; Neil et al., 2002). Among the functional pathways, laterality of the trace value was most asymmetric in the corticospinal tract (10% difference in term-born and 11% difference in preterm-born infants, right > left), followed by the optic radiation (4% difference in both term- and preterm-born infants, right > left). The asymmetry in the pathway connecting the sensory thalamus and the primary somatosensory cortex (2% difference, left > right) was seen only in term-born infants, and that in the inferior fronto-occipital fasciculus was seen only in preterm-born infants (3% difference, right > left). Since the strong laterality in the corticospinal tract has been reported in various age ranges, including healthy preterm-born neonates (Liu et al., 2010), infants (Dubois et al., 2009), and adults (Guye et al., 2003), this anatomical laterality might represent a physiological or functional laterality that exists from early development, although the relationship with handedness is still controversial (Seizeur et al., 2014; Westerhausen et al., 2007). Our results further validate the existence of such laterality by the neonatal period.

Laterality in the optic radiation was also reported in children, youth, and adults; however, the direction varied in different parts of the optic radiation (Kang et al., 2011; Park et al., 2004; Takao et al., 2011; Thiebaut de Schotten et al., 2011; Xie et al., 2007). Our findings are consistent with a prior study of children and youth that found left lateralization of FA

values due to a higher first eigenvalue, suggesting a lower axon density in the left hemisphere (Dayan et al., 2015). As myelination of the optic radiation is mature by three years of age (Brown et al., 2014), a two- to three-year longitudinal follow-up of our cohort is needed to investigate changes in diffusion measures over the latter phase of maturation.

Laterality in somatosensory-related pathways and the inferior fronto-occipital fasciculus has not been clearly established. A study of 6 −17-year-old adolescents found no laterality in FA or mean diffusivity (= trace/3) of the tract that connects the medial lemniscus and postcentral gyrus (Eluvathingal et al., 2007). Consistent with our findings, adults also showed a trend toward lower FA and higher mean diffusivity in the left side of the medial lemniscus at the brainstem (Kamali et al., 2009). No sex differences in diffusivity measures were observed in any fiber pathways in either term-born or preterm-born infants, consistent with a prior cross-sectional study of neonates (Oishi et al., 2011c). However, since sexual dimorphism is prominent in many white matter tracts, including the left cingulum bundle and the right inferior fronto-orbital fasciculus of young children (Johnson et al., 2013), a longitudinal follow-up of our neonatal cohort is needed to investigate early and late maturation of fiber tract laterality and sexual dimorphism.

4.3 Effect of preterm birth

The trace values of the preterm-born group were significantly higher than those of the term-born group in several structures, including the body of the CC, the left ILF, and the left V1/V2 – V5/MT+, and across all three time-points. Moreover, trace values (corrected for age in postmenstrual weeks at the time of the scan) were negatively correlated with gestational age at birth for the first and second time-points. These findings indicate that more severe prematurity is associated with more pronounced alterations in brain measures for these regions. Less or lack of such correlation at the final time-point suggested that the fiber tract maturation tends to normalize despite prematurity at birth, although the interaction between group (term or preterm) and time points was not significant. Several preterm-born infants showed persistently higher trace values than those of term-born babies, and 40 – 50% of these infants suffered from ROP, which was a higher percentage than the incidence of ROP in our entire preterm cohort (26.7%). This finding suggests an underlying pathological process that might have caused both ROP and white matter injury. Additional follow-up evaluations are needed to determine whether the persistently elevated trace values in specific functional pathways can predict future neurological deficits.

Preterm birth adversely affects neurological development in neonates (Atkinson and Braddick, 2007; Cheon et al., 2011; Fryer et al., 2008; Ortibus et al., 2012; Van Braeckel et al., 2008; Volpe, 2009). In long-term follow-up studies of preterm-born subjects with very-low-birth-weight, several white matter tracts, including the CC, the external capsule, the posterior part of the internal capsule, and the ILF, showed reduced anisotropy and elevated mean diffusivity at adolescence and early adulthood (Eikenes et al., 2011; Reveley et al., 2015; Skranes et al., 2007). Reduced FA was mostly found in those with a lower intelligent quotient, but not in those with a normal intelligent quotient, which indicated a functional relationship between the brain microstructure and cognition (Eikenes et al., 2011). Our findings, together with previous studies, suggest that abnormalities in white matter pathways

tend to normalize during early development, but insufficient recovery or additional underlying brain injury might be related to poorer functional outcomes.

4.4 Vulnerable white matter pathways in preterm birth and functional prediction

Abnormalities in the white matter pathways identified in this study corresponded to functional impairments in previous studies.

Higher diffusivity and lower FA in the CC have been reproducibly observed in preterm-born infants compared to term-born infants (Alexandrou et al., 2014; Anjari et al., 2007; Rose et al., 2008; Shim et al., 2012; Thompson et al., 2011), and severe abnormality was related to impaired motion and tonicity at a term-equivalent age (Mathew et al., 2013). Higher diffusivity in the CC at a term-equivalent age was associated with future impaired motor development, psychomotor delay, and tonicity (De Bruine et al., 2013; Thompson et al., 2012; Weinstein et al., 2014). These findings, based on retrospective DTI function-correlation studies, together with our findings, suggested that the abnormality of the CC in early development potentially predicts altered motor functions in later life. A prospective developmental evaluation of motor functions in our cohort is needed to confirm this predictive role.

The tracts ILF and V1/V2 – V5/MT+ are both related to visual function. Visual information from the retina is transferred to the primary visual cortex and split into two major streams (Goodale and Milner, 1992), the ventral visual stream, which projects from the primary visual area to V4 toward the temporal lobe via the ILF (Catani et al., 2003), and the dorsal visual stream, which projects from the primary visual area to V3A and to V5 through V1/V2 – V5/MT+, toward the parietal lobe. The ILF is known to be impaired in preterm-born individuals (Alexandrou et al., 2014; Salvan et al., 2014; Skranes et al., 2007) and the severity correlates with earlier birth (Salvan et al., 2014). A case series showed that the degree of injury in the ILF of five children (three born preterm) correlated with the severity of visual perception impairment (Ortibus et al., 2012). Since the ILF is involved in various functions related to visual processing (Chanraud et al., 2010) and the abnormalities in ILF have been reported in various diseases, such as schizophrenia with visual hallucinations (Ashtari et al., 2007) and Asperger's syndrome (Pugliese et al., 2009), the impairment seen in preterm-born infants could result in various functional disturbances. Visuomotor skills were often impaired in preterm-born children (Atkinson and Braddick, 2007; Van Braeckel et al., 2008), while motion response, measured by visual event-related potentials, was delayed in preterm-born infants (Atkinson and Braddick, 2007); both suggest an impaired dorsal visual stream, which is congruent with the altered V1/V2 – V5/MT+ demonstrated in our study. Dysfunction of the dorsal visual stream is known in diseases, such as Williams syndrome (Atkinson et al., 2001) and autistic spectrum disorder (Pellicano et al., 2005), and a relationship between the structural impairment and dysfunction in visual perception and visual-guided movement has been postulated (Philip and Dutton, 2014). The probabilistic map developed through this study has the potential to accelerate research in the field of visual processing by introducing a way to quantify anatomical abnormalities in the dorsal visual stream. Since the time-dependent decrease in trace values could be interpreted as an effect of the rapid reduction of water content and microstructural development during the

studied period, the higher trace values observed in preterm-born infants than in term-born infants could be interpreted as developmental delay or damage in the outgrowth of the axons, dendrites, or pre-oligodendrocytes of these structures (Volpe, 2009). The histopathological underpinnings of the selective vulnerability of the CC and visual pathway remain unknown (Huang et al., 2006; Trivedi et al., 2009b). Longitudinal analysis that begins at earlier postmenstrual weeks is anticipated to test a hypothesis that the area with rapid growth is vulnerable to the effect of prematurity (Estep et al., 2014).

4.5 Limitations

Our study has limitations. The misregistration of the cortical areas is a common problem when a single brain template is applied to parcellate infant brains with low tissue contrast, and this might cause artificial findings, although the Jülich cytoarchitectonic atlas, which is based on probability, could potentially ameliorate the issue in this study. We adopted the single template approach to use the Jülich cytoarchitectonic map on the Colin-27 brain. Since multi-atlas-based approaches with high parcellation accuracy have been recently developed, we expect that the creation of multiple cytoarchitectonic maps, combined with MRI and DTI, will be an important future direction. Such a multi-atlas resource could be combined with sophisticated image segmentation approaches, such as the learning-based multi-source integration framework (LINKS) (Wang et al., 2015), to improve the accuracy of cortical parcellation in the future. Since DP automatically connects two areas with the lowest cumulative cost of trajectory, false negative and positive fibers could potentially be generated, especially when highly aligned fibers are adjacent to the target fiber. Future applications may require further validation of these probabilistic maps with a larger sample of healthy infants and a wider age range. Although we chose a relatively high probabilistic threshold and applied visual quality control to quantify the diffusion measures of each pathway, the effects of partial volume might remain, which is a common problem in neuroimaging analyses. The differences in ethnicity and socioeconomic status between term-born and preterm-born infants could potentially affect the results, since ethnicity is known to affect the FA values of several structures, including the anterior limb of the internal capsule and the genu of the CC in neonates (Bai et al., 2012). In addition, lower income status during early development could reduce gray matter volume (Hanson et al., 2013). The effects on the functional pathways have yet to be elucidated. The clinical significance of higher trace values in several pathways of the preterm infants remains unknown since we have not correlated the trace values with later neurobehavioral and cognitive outcomes, which will be performed in future follow-up studies.

5. Conclusion

Probabilistic maps of white matter pathways with known associated functions were introduced to provide an opportunity to investigate developmental changes and the pathology of these pathways. Maturation patterns of these pathways were investigated through a longitudinal study of term-born and preterm-born neonates. We identified delayed development in the CC and the visual-related pathways in preterm-born infants. These probabilistic maps may be useful for early identification of delayed milestones in preterm-born infants.

Acknowledgments

This publication was made possible by grants R01HD065955, 2K24DA16170, U54NS056883, G12MD007601-26, P41EB015909 from the National Institutes of Health and grant 46039500 from the Central Norway Regional Health Authority, and research fellowship (to K. A.) from the Uehara Memorial Foundation. The contents of this paper are solely the responsibility of the authors and do not necessarily represent the official view of NIH, the Central Norway Regional Health Authority, or the Uehara Memorial Foundation. The authors are grateful to the families of our research participants, pediatricians/neonatologists (Dr. Lillian Fujimoto, Dr. Lois Chiu, and Dr. Joseph Hudak), and our research staff (Heather Johansen, Antonette Hernandez, and Caroline Jiang), who assisted with the data collection and data transfer. We also thank Ms. Mary McAllister for help with manuscript editing, Mr. Rajiv Deshpande for the technical support, Dr. Susumu Mori for advice about DTI scans, and Dr. Doris Lin for image reading and reporting as a neuroradiologist certified by the American Board of Neuroradiology. We would like to acknowledge partial support for the statistical analysis from the National Center for Research Resources and the National Center for Advancing Translational Sciences (NCATS) of the National Institutes of Health through Grant Number 1UL1TR001079, and the statistician of the Johns Hopkins Biostatistics Center, Ms. Carol B. Thompson.

Abbreviations

AAL	automated anatomical labeling
ABA	atlas-based analysis
DP	dynamic programming
DTI	diffusion tensor imaging
EPI	echo planar imaging
FA	fractional anisotropy
LDDMM	large deformation diffeomorphic metric mapping
MGB	medial geniculate body
RF	radio frequency
ROP	retinopathy of prematurity
SENSE	sensitivity encoding
SWM	superficial white matter
TBSS	tract-based spatial statistics
TOI	tracts-of-interest

References

Alexandrou G, Martensson G, Skiold B, Blennow M, Aden U, Vollmer B. White matter microstructure is influenced by extremely preterm birth and neonatal respiratory factors. Acta Paediatr. 2014; 103:48–56. [PubMed: 24118089]

Amunts K, Malikovic A, Mohlberg H, Schormann T, Zilles K. Brodmann's areas 17 and 18 brought into stereotaxic space-where and how variable? Neuroimage. 2000; 11:66–84. [PubMed: 10686118]

Anjari M, Srinivasan L, Allsop JM, Hajnal JV, Rutherford MA, Edwards AD, Counsell SJ. Diffusion tensor imaging with tract-based spatial statistics reveals local white matter abnormalities in preterm infants. Neuroimage. 2007; 35:1021–1027. [PubMed: 17344066]

Ashtari M, Cottone J, Ardekani BA, Cervellione K, Szeszko PR, Wu J, Chen S, Kumra S. Disruption of white matter integrity in the inferior longitudinal fasciculus in adolescents with schizophrenia as revealed by fiber tractography. Arch Gen Psychiatry. 2007; 64:1270–1280. [PubMed: 17984396]

Atkinson J, Anker S, Braddick O, Nokes L, Mason A, Braddick F. Visual and visuospatial development in young children with Williams syndrome. Dev Med Child Neurol. 2001; 43:330–337. [PubMed: 11368486]

Atkinson J, Braddick O. Visual and visuocognitive development in children born very prematurely. Prog Brain Res. 2007; 164:123–149. [PubMed: 17920429]

Bai J, Abdul-Rahman MF, Rifkin-Graboi A, Chong YS, Kwek K, Saw SM, Godfrey KM, Gluckman PD, Fortier MV, Meaney MJ, Qiu A. Population differences in brain morphology and microstructure among Chinese, Malay, and Indian neonates. PLoS One. 2012; 7:e47816. [PubMed: 23112850]

Ball G, Counsell SJ, Anjari M, Merchant N, Arichi T, Doria V, Rutherford MA, Edwards AD, Rueckert D, Boardman JP. An optimised tract-based spatial statistics protocol for neonates: applications to prematurity and chronic lung disease. Neuroimage. 2010; 53:94–102. [PubMed: 20510375]

Bammer R, Keeling SL, Auer M, Pruessmann KP, Roeschmann P, Stollberger R, Hartung HP, Fazekas F. Diffusion tensor imaging using SENSE-single-shot EPI. International Society of Magnetic Resonance in Medicine. Glasgow. 2001:160.

Baumann N, Pham-Dinh D. Biology of oligodendrocyte and myelin in the mammalian central nervous system. Physiol Rev. 2001; 81:871–927. [PubMed: 11274346]

Berman JI, Lanza MR, Blaskey L, Edgar JC, Roberts TP. High angular resolution diffusion imaging probabilistic tractography of the auditory radiation. AJNR Am J Neuroradiol. 2013; 34:1573–1578. [PubMed: 23493892]

Braga RM, Roze E, Ball G, Merchant N, Tusor N, Arichi T, Edwards D, Rueckert D, Counsell SJ. Development of the Corticospinal and Callosal Tracts from Extremely Premature Birth up to 2 Years of Age. PLoS One. 2015; 10:e0125681. [PubMed: 25955638]

Brown CJ, Miller SP, Booth BG, Andrews S, Chau V, Poskitt KJ, Hamarneh G. Structural network analysis of brain development in young preterm neonates. Neuroimage. 2014; 101:667–680. [PubMed: 25076107]

Catani M, Jones DK, Donato R, Ffytche DH. Occipito-temporal connections in the human brain. Brain. 2003; 126:2093–2107. [PubMed: 12821517]

Ceritoglu C, Oishi K, Li X, Chou MC, Younes L, Albert M, Lyketsos C, van Zijl PC, Miller MI, Mori S. Multi-contrast large deformation diffeomorphic metric mapping for diffusion tensor imaging. Neuroimage. 2009; 47:618–627. [PubMed: 19398016]

Chang L, Akazawa K, Yamakawa R, Hayama S, Buchthal S, Alicata D, Andres T, Castillo D, Oishi K, Skranes J, Ernst T, Oishi K, submitted. Delayed early developmental trajectories of white matter tracts of functional pathways in preterm-born infants measured by longitudinal diffusion tensor imaging. Data in Brief.

Chanraud S, Zahr N, Sullivan EV, Pfefferbaum A. MR diffusion tensor imaging: a window into white matter integrity of the working brain. Neuropsychol Rev. 2010; 20:209–225. [PubMed: 20422451]

Cheon KA, Kim YS, Oh SH, Park SY, Yoon HW, Herrington J, Nair A, Koh YJ, Jang DP, Kim YB, Leventhal BL, Cho ZH, Castellanos FX, Schultz RT. Involvement of the anterior thalamic radiation in boys with high functioning autism spectrum disorders: a Diffusion Tensor Imaging study. Brain Res. 2011; 1417:77–86. [PubMed: 21890117]

Dayan M, Munoz M, Jentschke S, Chadwick MJ, Cooper JM, Riney K, Vargha-Khadem F, Clark CA. Optic radiation structure and anatomy in the normally developing brain determined using diffusion MRI and tractography. Brain Struct Funct. 2015; 220:291–306. [PubMed: 24170375]

De Bruine FT, Van Wezel-Meijler G, Leijser LM, Steggerda SJ, Van Den Berg-Huysmans AA, Rijken M, Van Buchem MA, Van Der Grond J. Tractography of white-matter tracts in very preterm infants: a 2-year follow-up study. Dev Med Child Neurol. 2013; 55:427–433. [PubMed: 23441853]

Dubois J, Dehaene-Lambertz G, Perrin M, Mangin JF, Cointepas Y, Duchesnay E, Le Bihan D, Hertz-Pannier L. Asynchrony of the early maturation of white matter bundles in healthy infants: quantitative landmarks revealed noninvasively by diffusion tensor imaging. Hum Brain Mapp. 2008; 29:14–27. [PubMed: 17318834]

Dubois J, Hertz-Pannier L, Dehaene-Lambertz G, Cointepas Y, Le Bihan D. Assessment of the early organization and maturation of infants' cerebral white matter fiber bundles: a feasibility study using quantitative diffusion tensor imaging and tractography. Neuroimage. 2006; 30:1121–1132. [PubMed: 16413790]

Dubois J, Hertz-Pannier L, Cachia A, Mangin JF, Le Bihan D, Dehaene-Lambertz G. Structural asymmetries in the infant language and sensori-motor networks. Cereb Cortex. 2009; 19:414–423. [PubMed: 18562332]

Eickhoff SB, Stephan KE, Mohlberg H, Grefkes C, Fink GR, Amunts K, Zilles K. A new SPM toolbox for combining probabilistic cytoarchitectonic maps and functional imaging data. Neuroimage. 2005; 25:1325–1335. [PubMed: 15850749]

Eikenes L, Lohaugen GC, Brubakk AM, Skranes J, Haberg AK. Young adults born preterm with very low birth weight demonstrate widespread white matter alterations on brain DTI. Neuroimage. 2011; 54:1774–1785. [PubMed: 20965255]

Eluvathingal TJ, Hasan KM, Kramer L, Fletcher JM, Ewing-Cobbs L. Quantitative diffusion tensor tractography of association and projection fibers in normally developing children and adolescents. Cereb Cortex. 2007; 17:2760–2768. [PubMed: 17307759]

Estep ME, Smyser CD, Anderson PJ, Ortinau CM, Wallendorf M, Katzman CS, Doyle LW, Thompson DK, Neil JJ, Inder TE, Shimony JS. Diffusion tractography and neuromotor outcome in very preterm children with white matter abnormalities. Pediatr Res. 2014; 76:86–92. [PubMed: 24713814]

Fryer SL, Frank LR, Spadoni AD, Theilmann RJ, Nagel BJ, Schweinsburg AD, Tapert SF. Microstructural integrity of the corpus callosum linked with neuropsychological performance in adolescents. Brain Cogn. 2008; 67:225–233. [PubMed: 18346830]

Gao J, Li X, Hou X, Ding A, Chan KC, Sun Q, Wu EX, Yang J. Tract-based spatial statistics (TBSS): application to detecting white matter tract variation in mild hypoxic-ischemic neonates. Conf Proc IEEE Eng Med Biol Soc. 2012; 2012:432–435. [PubMed: 23365921]

Gao W, Lin W, Chen Y, Gerig G, Smith JK, Jewells V, Gilmore JH. Temporal and spatial development of axonal maturation and myelination of white matter in the developing brain. AJNR Am J Neuroradiol. 2009; 30:290–296. [PubMed: 19001533]

Geyer S. The microstructural border between the motor and the cognitive domain in the human cerebral cortex. Adv Anat Embryol Cell Biol. 2004; 174(I-VIII):1–89.

Geyer S, Ledberg A, Schleicher A, Kinomura S, Schormann T, Burgel U, Klingberg T, Larsson J, Zilles K, Roland PE. Two different areas within the primary motor cortex of man. Nature. 1996; 382:805–807. [PubMed: 8752272]

Geyer S, Schleicher A, Zilles K. Areas 3a, 3b, and 1 of human primary somatosensory cortex. Neuroimage. 1999; 10:63–83. [PubMed: 10385582]

Geyer S, Schormann T, Mohlberg H, Zilles K. Areas 3a, 3b, and 1 of human primary somatosensory cortex. Part 2. Spatial normalization to standard anatomical space. Neuroimage. 2000; 11:684–696. [PubMed: 10860796]

Gilmore JH, Lin W, Corouge I, Vetsa YS, Smith JK, Kang C, Gu H, Hamer RM, Lieberman JA, Gerig G. Early postnatal development of corpus callosum and corticospinal white matter assessed with quantitative tractography. AJNR Am J Neuroradiol. 2007; 28:1789–1795. [PubMed: 17923457]

Goodale MA, Milner AD. Separate visual pathways for perception and action. Trends Neurosci. 1992; 15:20–25. [PubMed: 1374953]

Grefkes C, Geyer S, Schormann T, Roland P, Zilles K. Human somatosensory area 2: observer-independent cytoarchitectonic mapping, interindividual variability, and population map. Neuroimage. 2001; 14:617–631. [PubMed: 11506535]

Guye M, Parker GJ, Symms M, Boulby P, Wheeler-Kingshott CA, Salek-Haddadi A, Barker GJ, Duncan JS. Combined functional MRI and tractography to demonstrate the connectivity of the human primary motor cortex in vivo. Neuroimage. 2003; 19:1349–1360. [PubMed: 12948693]

Hanson JL, Hair N, Shen DG, Shi F, Gilmore JH, Wolfe BL, Pollak SD. Family poverty affects the rate of human infant brain growth. PLoS One. 2013; 8:e80954. [PubMed: 24349025]

Holland D, Chang L, Ernst TM, Curran M, Buchthal SD, Alicata D, Skranes J, Johansen H, Hernandez A, Yamakawa R, Kuperman JM, Dale AM. Structural growth trajectories and rates of change in

the first 3 months of infant brain development. JAMA Neurol. 2014; 71:1266–1274. [PubMed: 25111045]

Holmes CJ, Hoge R, Collins L, Woods R, Toga AW, Evans AC. Enhancement of MR images using registration for signal averaging. J Comput Assist Tomogr. 1998; 22:324–333. [PubMed: 9530404]

Huang H, Zhang J, Wakana S, Zhang W, Ren T, Richards LJ, Yarowsky P, Donohue P, Graham E, van Zijl PC, Mori S. White and gray matter development in human fetal, newborn and pediatric brains. Neuroimage. 2006; 33:27–38. [PubMed: 16905335]

Huppi PS, Maier SE, Peled S, Zientara GP, Barnes PD, Jolesz FA, Volpe JJ. Microstructural development of human newborn cerebral white matter assessed in vivo by diffusion tensor magnetic resonance imaging. Pediatr Res. 1998; 44:584–590. [PubMed: 9773850]

Jaermann T, Crelier G, Pruessmann KP, Golay X, Netsch T, van Muiswinkel AM, Mori S, van Zijl PC, Valavanis A, Kollias S, Boesiger P. SENSE-DTI at 3 T. Magn Reson Med. 2004; 51:230–236. [PubMed: 14755645]

Jiang H, van Zijl PC, Kim J, Pearlson GD, Mori S. DtiStudio: resource program for diffusion tensor computation and fiber bundle tracking. Comput Methods Programs Biomed. 2006; 81:106–116. [PubMed: 16413083]

Johnson RT, Yeatman JD, Wandell BA, Buonocore MH, Amaral DG, Nordahl CW. Diffusion properties of major white matter tracts in young, typically developing children. Neuroimage. 2013; 88C:143–154. [PubMed: 24269274]

Jones DK, Horsfield MA, Simmons A. Optimal strategies for measuring diffusion in anisotropic systems by magnetic resonance imaging. Magn. Reson Med. 1999; 42:515–525. [PubMed: 10467296]

Kamali A, Kramer LA, Butler IJ, Hasan KM. Diffusion tensor tractography of the somatosensory system in the human brainstem: initial findings using high isotropic spatial resolution at 3.0 T. Eur Radiol. 2009; 19:1480–1488. [PubMed: 19189108]

Kang X, Herron TJ, Woods DL. Regional variation, hemispheric asymmetries and gender differences in pericortical white matter. Neuroimage. 2011; 56:2011–2023. [PubMed: 21397700]

Kaur S, Powell S, He L, Pierson CR, Parikh NA. Reliability and repeatability of quantitative tractography methods for mapping structural white matter connectivity in preterm and term infants at term-equivalent age. PLoS One. 2014; 9:e85807. [PubMed: 24475054]

Kersbergen KJ, Leemans A, Groenendaal F, van der Aa NE, Viergever MA, de Vries LS, Benders MJ. Microstructural brain development between 30 and 40 weeks corrected age in a longitudinal cohort of extremely preterm infants. Neuroimage. 2014; 103:214–224. [PubMed: 25261000]

Khaneja N, Miller MI, Grenander U. Dynamic programming generation of geodesics and sulci on brain surfaces. IEEE Trans. Pattern Anal. Mach. Intell. 1998; 20:1260–1265.

Kinney HC, Brody BA, Kloman AS, Gilles FH. Sequence of central nervous system myelination in human infancy. II. Patterns of myelination in autopsied infants. J Neuropathol Exp Neurol. 1988; 47:217–234. [PubMed: 3367155]

Kuklisova-Murgasova M, Aljabar P, Srinivasan L, Counsell SJ, Doria V, Serag A, Gousias IS, Boardman JP, Rutherford MA, Edwards AD, Hajnal JV, Rueckert D. A dynamic 4D probabilistic atlas of the developing brain. Neuroimage. 2011; 54:2750–2763. [PubMed: 20969966]

Lepomaki V, Matomaki J, Lapinleimu H, Lehtonen L, Haataja L, Komu M, Parkkola R. Effect of antenatal growth on brain white matter maturation in preterm infants at term using tract-based spatial statistics. Pediatr Radiol. 2013; 43:80–85. [PubMed: 23160647]

Li M, Ratnanather JT, Miller MI, Mori S. Knowledge-based automated reconstruction of human brain white matter tracts using a path-finding approach with dynamic programming. Neuroimage. 2014; 88:271–281. [PubMed: 24135166]

Liu Y, Baleriaux D, Kavec M, Metens T, Absil J, Denolin V, Pardou A, Avni F, Van Bogaert P, Aeby A. Structural asymmetries in motor and language networks in a population of healthy preterm neonates at term equivalent age: a diffusion tensor imaging and probabilistic tractography study. Neuroimage. 2010; 51:783–788. [PubMed: 20206706]

Loh KB, Ramli N, Tan LK, Roziah M, Rahmat K, Ariffin H. Quantification of diffusion tensor imaging in normal white matter maturation of early childhood using an automated processing pipeline. Eur Radiol. 2012; 22:1413–1426. [PubMed: 22434420]

Malikovic A, Amunts K, Schleicher A, Mohlberg H, Eickhoff SB, Wilms M, Palomero-Gallagher N, Armstrong E, Zilles K. Cytoarchitectonic analysis of the human extrastriate cortex in the region of V5/MT+: a probabilistic, stereotaxic map of area hOc5. Cereb Cortex. 2007; 17:562–574. [PubMed: 16603710]

Mathew P, Pannek K, Snow P, D'Acunto MG, Guzzetta A, Rose SE, Colditz PB, Finnigan S. Maturation of corpus callosum anterior midbody is associated with neonatal motor function in eight preterm-born infants. Neural Plast. 2013; 2013:359532. [PubMed: 23509639]

Miller SP, McQuillen PS, Hamrick S, Xu D, Glidden DV, Charlton N, Karl T, Azakie A, Ferriero DM, Barkovich AJ, Vigneron DB. Abnormal brain development in newborns with congenital heart disease. N Engl J Med. 2007; 357:1928–1938. [PubMed: 17989385]

Miller SP, Vigneron DB, Henry RG, Bohland MA, Ceppi-Cozzio C, Hoffman C, Newton N, Partridge JC, Ferriero DM, Barkovich AJ. Serial quantitative diffusion tensor MRI of the premature brain: development in newborns with and without injury. J Magn Reson Imaging. 2002; 16:621–632. [PubMed: 12451575]

Mori S, Crain BJ, Chacko VP, van Zijl PC. Three-dimensional tracking of axonal projections in the brain by magnetic resonance imaging. Ann Neurol. 1999; 45:265–269. [PubMed: 9989633]

Mori S, Oishi K, Jiang H, Jiang L, Li X, Akhter K, Hua K, Faria AV, Mahmood A, Woods R, Toga AW, Pike GB, Neto PR, Evans A, Zhang J, Huang H, Miller MI, van Zijl P, Mazziotta J. Stereotaxic white matter atlas based on diffusion tensor imaging in an ICBM template. Neuroimage. 2008; 40:570–582. [PubMed: 18255316]

Morosan P, Rademacher J, Schleicher A, Amunts K, Schormann T, Zilles K. Human primary auditory cortex: cytoarchitectonic subdivisions and mapping into a spatial reference system. Neuroimage. 2001; 13:684–701. [PubMed: 11305897]

Mourmans J, Majoie CB, Barth PG, Duran M, Akkerman EM, Poll-The BT. Sequential MR imaging changes in nonketotic hyperglycinemia. AJNR Am J Neuroradiol. 2006; 27:208–211. [PubMed: 16418385]

Mukherjee P, Miller JH, Shimony JS, Conturo TE, Lee BC, Almli CR, McKinstry RC. Normal brain maturation during childhood: developmental trends characterized with diffusion-tensor MR imaging. Radiology. 2001; 221:349–358. [PubMed: 11687675]

Mukherjee P, Miller JH, Shimony JS, Philip JV, Nehra D, Snyder AZ, Conturo TE, Neil JJ, McKinstry RC. Diffusion-tensor MR imaging of gray and white matter development during normal human brain maturation. AJNR Am J Neuroradiol. 2002; 23:1445–1456. [PubMed: 12372731]

Neil J, Miller J, Mukherjee P, Huppi PS. Diffusion tensor imaging of normal and injured developing human brain - a technical review. NMR Biomed. 2002; 15:543–552. [PubMed: 12489100]

Nijman J, Gunkel J, de Vries LS, van Kooij BJ, van Haastert IC, Benders MJ, Kersbergen KJ, Verboon-Maciolek MA, Groenendaal F. Reduced occipital fractional anisotropy on cerebral diffusion tensor imaging in preterm infants with postnatally acquired cytomegalovirus infection. Neonatology. 2013; 104:143–150. [PubMed: 23887677]

O'Gorman RL, Bucher HU, Held U, Koller BM, Huppi PS, Hagmann CF, Swiss EPONTG. Tract-based spatial statistics to assess the neuroprotective effect of early erythropoietin on white matter development in preterm infants. Brain. 2015; 138:388–397. [PubMed: 25534356]

Oishi K, Akhter K, Mielke M, Ceritoglu C, Zhang J, Jiang H, Li X, Younes L, Miller MI, van Zijl PC, Albert M, Lyketsos CG, Mori S. Multi-modal MRI analysis with disease-specific spatial filtering: initial testing to predict mild cognitive impairment patients who convert to Alzheimer's disease. Front Neurol. 2011a; 2:54. [PubMed: 21904533]

Oishi K, Faria A, Jiang H, Li X, Akhter K, Zhang J, Hsu JT, Miller MI, van Zijl PC, Albert M, Lyketsos CG, Woods R, Toga AW, Pike GB, Rosa-Neto P, Evans A, Mazziotta J, Mori S. Atlas-based whole brain white matter analysis using large deformation diffeomorphic metric mapping: application to normal elderly and Alzheimer's disease participants. Neuroimage. 2009; 46:486–499. [PubMed: 19385016]

Oishi K, Faria AV, Mori S. Advanced neonatal NeuroMRI. Magn Reson Imaging Clin N Am. 2012; 20:81–91. [PubMed: 22118594]

Oishi K, Faria AV, Yoshida S, Chang L, Mori S. Quantitative evaluation of brain development using anatomical MRI and diffusion tensor imaging. Int J Dev Neurosci. 2013; 31:512–524. [PubMed: 23796902]

Oishi K, Huang H, Yoshioka T, Ying SH, Zee DS, Zilles K, Amunts K, Woods R, Toga AW, Pike GB, Rosa-Neto P, Evans AC, van Zijl PC, Mazziotta JC, Mori S. Superficially located white matter structures commonly seen in the human and the macaque brain with diffusion tensor imaging. Brain Connect. 2011b; 1:37–47. [PubMed: 22432953]

Oishi K, Mori S, Donohue PK, Ernst T, Anderson L, Buchthal S, Faria A, Jiang H, Li X, Miller MI, van Zijl PC, Chang L. Multi-contrast human neonatal brain atlas: application to normal neonate development analysis. Neuroimage. 2011c; 56:8–20. [PubMed: 21276861]

Oishi K, Zilles K, Amunts K, Faria A, Jiang H, Li X, Akhter K, Hua K, Woods R, Toga AW, Pike GB, Rosa-Neto P, Evans A, Zhang J, Huang H, Miller MI, van Zijl PC, Mazziotta J, Mori S. Human brain white matter atlas: identification and assignment of common anatomical structures in superficial white matter. Neuroimage. 2008; 43:447–457. [PubMed: 18692144]

Okumura A, Hayakawa M, Tsuji T, Naganawa S, Watanabe K. Diffusion tensor imaging in infants with basal ganglia-thalamic lesions. Eur J Paediatr Neurol. 2008; 12:412–416. [PubMed: 18061499]

Ortibus E, Verhoeven J, Sunaert S, Casteels I, de Cock P, Lagae L. Integrity of the inferior longitudinal fasciculus and impaired object recognition in children: a diffusion tensor imaging study. Dev Med Child Neurol. 2012; 54:38–43. [PubMed: 22171928]

Padilla N, Junque C, Figueras F, Sanz-Cortes M, Bargallo N, Arranz A, Donaire A, Figueras J, Gratacos E. Differential vulnerability of gray matter and white matter to intrauterine growth restriction in preterm infants at 12 months corrected age. Brain Res. 2014; 1545:1–11. [PubMed: 24361462]

Panigrahy A, Bluml S. Advances in magnetic resonance neuroimaging techniques in the evaluation of neonatal encephalopathy. Top Magn Reson Imaging. 2007; 18:3–29. [PubMed: 17607141]

Pannek K, Hatzigeorgiou X, Colditz PB, Rose S. Assessment of structural connectivity in the preterm brain at term equivalent age using diffusion MRI and T2 relaxometry: a network-based analysis. PLoS One. 2013; 8:e68593. [PubMed: 23950872]

Paquette LB, Wisnowski JL, Ceschin R, Pruetz JD, Detterich JA, Del Castillo S, Nagasunder AC, Kim R, Painter MJ, Gilles FH, Nelson MD, Williams RG, Bluml S, Panigrahy A. Abnormal cerebral microstructure in premature neonates with congenital heart disease. AJNR Am J Neuroradiol. 2013; 34:2026–2033. [PubMed: 23703146]

Park HJ, Westin CF, Kubicki M, Maier SE, Niznikiewicz M, Baer A, Frumin M, Kikinis R, Jolesz FA, McCarley RW, Shenton ME. White matter hemisphere asymmetries in healthy subjects and in schizophrenia: a diffusion tensor MRI study. Neuroimage. 2004; 23:213–223. [PubMed: 15325368]

Parmar H, Sitoh YY, Ho L. Maple syrup urine disease: diffusion-weighted and diffusion-tensor magnetic resonance imaging findings. J Comput Assist Tomogr. 2004; 28:93–97. [PubMed: 14716239]

Pellicano E, Gibson L, Maybery M, Durkin K, Badcock DR. Abnormal global processing along the dorsal visual pathway in autism: a possible mechanism for weak visuospatial coherence? Neuropsychologia. 2005; 43:1044–1053. [PubMed: 15769490]

Philip SS, Dutton GN. Identifying and characterising cerebral visual impairment in children: a review. Clin Exp Optom. 2014; 97:196–208. [PubMed: 24766507]

Pierpaoli C, Barnett A, Pajevic S, Chen R, Penix LR, Virta A, Basser P. Water diffusion changes in Wallerian degeneration and their dependence on white matter architecture. Neuroimage. 2001; 13:1174–1185. [PubMed: 11352623]

Pogribna U, Yu X, Burson K, Zhou Y, Lasky RE, Narayana PA, Parikh NA. Perinatal clinical antecedents of white matter microstructural abnormalities on diffusion tensor imaging in extremely preterm infants. PLoS One. 2013; 8:e72974. [PubMed: 24009724]

Porter EJ, Counsell SJ, Edwards AD, Allsop J, Azzopardi D. Tract-based spatial statistics of magnetic resonance images to assess disease and treatment effects in perinatal asphyxial encephalopathy. Pediatr Res. 2010; 68:205–209. [PubMed: 20520585]

Prayer D, Barkovich AJ, Kirschner DA, Prayer LM, Roberts TP, Kucharczyk J, Moseley ME. Visualization of nonstructural changes in early white matter development on diffusion-weighted MR images: evidence supporting premyelination anisotropy. AJNR Am J Neuroradiol. 2001; 22:1572–1576. [PubMed: 11559509]

Provenzale JM, Liang L, DeLong D, White LE. Diffusion tensor imaging assessment of brain white matter maturation during the first postnatal year. AJR Am J Roentgenol. 2007; 189:476–486. [PubMed: 17646476]

Pruessmann KP, Weiger M, Scheidegger MB, Boesiger P. SENSE: sensitivity encoding for fast MRI. Magn Reson Med. 1999; 42:952–962. [PubMed: 10542355]

Pugliese L, Catani M, Ameis S, Dell'Acqua F, Thiebaut de Schotten M, Murphy C, Robertson D, Deeley Q, Daly E, Murphy DG. The anatomy of extended limbic pathways in Asperger syndrome: a preliminary diffusion tensor imaging tractography study. Neuroimage. 2009; 47:427–434. [PubMed: 19446642]

Ratnanather JT, Barta PE, Honeycutt NA, Lee N, Morris HM, Dziorny AC, Hurdal MK, Pearlson GD, Miller MI. Dynamic programming generation of boundaries of local coordinatized submanifolds in the neocortex: application to the planum temporale. Neuroimage. 2003; 20:359–377. [PubMed: 14527596]

Ratnanather JT, Lal RM, An M, Poynton CB, Li M, Jiang H, Oishi K, Selemon LD, Mori S, Miller MI. Cortico-cortical, cortico-striatal, and cortico-thalamic white matter fiber tracts generated in the macaque brain via dynamic programming. Brain Connect. 2013; 3:475–490. [PubMed: 23879573]

Reveley C, Seth AK, Pierpaoli C, Silva AC, Yu D, Saunders RC, Leopold DA, Ye FQ. Superficial white matter fiber systems impede detection of long-range cortical connections in diffusion MR tractography. Proc Natl Acad Sci U S A. 2015; 112:E2820–E2828. [PubMed: 25964365]

Rose J, Vassar R, Cahill-Rowley K, Guzman XS, Stevenson DK, Barnea-Goraly N. Brain microstructural development at near-term age in very-low-birth-weight preterm infants: an atlas-based diffusion imaging study. Neuroimage. 2014a; 86:244–256. [PubMed: 24091089]

Rose J, Vassar R, Cahill-Rowley K, Stecher Guzman X, Hintz SR, Stevenson DK, Barnea-Goraly N. Neonatal physiological correlates of near-term brain development on MRI and DTI in very-low-birth-weight preterm infants. Neuroimage Clin. 2014b; 5:169–177. [PubMed: 25068107]

Rose SE, Hatzigeorgiou X, Strudwick MW, Durbridge G, Davies PS, Colditz PB. Altered white matter diffusion anisotropy in normal and preterm infants at term-equivalent age. Magn Reson Med. 2008; 60:761–767. [PubMed: 18816850]

Saksena S, Husain N, Malik GK, Trivedi R, Sarma M, Rathore RS, Pandey CM, Gupta RK. Comparative evaluation of the cerebral and cerebellar white matter development in pediatric age group using quantitative diffusion tensor imaging. Cerebellum. 2008; 7:392–400. [PubMed: 18581196]

Salvan P, Froudist Walsh S, Allin MP, Walshe M, Murray RM, Bhattacharyya S, McGuire PK, Williams SC, Nosarti C. Road work on memory lane--functional and structural alterations to the learning and memory circuit in adults born very preterm. Neuroimage 102 Pt. 2014; 1:152–161.

Schmahmann, JD.; Pandya, DN. Fiber Pathways of the Brain. New York: Oxford University Press; 2006.

Seizeur R, Magro E, Prima S, Wiest-Daessle N, Maumet C, Morandi X. Corticospinal tract asymmetry and handedness in right- and left-handers by diffusion tensor tractography. Surg Radiol Anat. 2014; 36:111–124. [PubMed: 23807198]

Serag A, Aljabar P, Ball G, Counsell SJ, Boardman JP, Rutherford MA, Edwards AD, Hajnal JV, Rueckert D. Construction of a consistent high-definition spatio-temporal atlas of the developing brain using adaptive kernel regression. Neuroimage. 2012; 59:2255–2265. [PubMed: 21985910]

Shi F, Wang L, Wu G, Li G, Gilmore JH, Lin W, Shen D. Neonatal atlas construction using sparse representation. Hum Brain Mapp. 2014; 35:4663–4677. [PubMed: 24638883]

Shim SY, Jeong HJ, Son DW, Jeong JS, Oh SH, Park SY, Ryu TH, Kim YB, Cho ZH. Altered microstructure of white matter except the corpus callosum is independent of prematurity. Neonatology. 2012; 102:309–315. [PubMed: 22986463]

Skranes J, Vangberg TR, Kulseng S, Indredavik MS, Evensen KA, Martinussen M, Dale AM, Haraldseth O, Brubakk AM. Clinical findings and white matter abnormalities seen on diffusion tensor imaging in adolescents with very low birth weight. Brain. 2007; 130:654–666. [PubMed: 17347255]

Smith SM, Jenkinson M, Johansen-Berg H, Rueckert D, Nichols TE, Mackay CE, Watkins KE, Ciccarelli O, Cader MZ, Matthews PM, Behrens TE. Tract-based spatial statistics: voxelwise analysis of multi-subject diffusion data. Neuroimage. 2006; 31:1487–1505. [PubMed: 16624579]

Takao H, Abe O, Yamasue H, Aoki S, Sasaki H, Kasai K, Yoshioka N, Ohtomo K. Gray and white matter asymmetries in healthy individuals aged 21–29 years: a voxel-based morphometry and diffusion tensor imaging study. Hum Brain Mapp. 2011; 32:1762–1773. [PubMed: 20886579]

Taylor PA, Jacobson SW, van der Kouwe A, Molteno CD, Chen G, Wintermark P, Alhamud A, Jacobson JL, Meintjes EM. A DTI-based tractography study of effects on brain structure associated with prenatal alcohol exposure in newborns. Hum Brain Mapp. 2015; 36:170–186. [PubMed: 25182535]

Thiebaut de Schotten M, Ffytche DH, Bizzi A, Dell'Acqua F, Allin M, Walshe M, Murray R, Williams SC, Murphy DG, Catani M. Atlasing location, asymmetry and inter-subject variability of white matter tracts in the human brain with MR diffusion tractography. Neuroimage. 2011; 54:49–59. [PubMed: 20682348]

Thompson DK, Inder TE, Faggian N, Johnston L, Warfield SK, Anderson PJ, Doyle LW, Egan GF. Characterization of the corpus callosum in very preterm and full-term infants utilizing MRI. Neuroimage. 2011; 55:479–490. [PubMed: 21168519]

Thompson DK, Inder TE, Faggian N, Warfield SK, Anderson PJ, Doyle LW, Egan GF. Corpus callosum alterations in very preterm infants: perinatal correlates and 2 year neurodevelopmental outcomes. Neuroimage. 2012; 59:3571–3581. [PubMed: 22154956]

Trivedi R, Agarwal S, Rathore RK, Saksena S, Tripathi RP, Malik GK, Pandey CM, Gupta RK. Understanding development and lateralization of major cerebral fiber bundles in pediatric population through quantitative diffusion tensor tractography. Pediatr Res. 2009a; 66:636–641. [PubMed: 19687778]

Trivedi R, Gupta RK, Husain N, Rathore RK, Saksena S, Srivastava S, Malik GK, Das V, Pradhan M, Sarma MK, Pandey CM, Narayana PA. Region-specific maturation of cerebral cortex in human fetal brain: diffusion tensor imaging and histology. Neuroradiology. 2009b; 51:567–576. [PubMed: 19421746]

Tzourio-Mazoyer N, Landeau B, Papathanassiou D, Crivello F, Etard O, Delcroix N, Mazoyer B, Joliot M. Automated anatomical labeling of activations in SPM using a macroscopic anatomical parcellation of the MNI MRI single-subject brain. Neuroimage. 2002; 15:273–289. [PubMed: 11771995]

Van Braeckel K, Butcher PR, Geuze RH, van Duijn MA, Bos AF, Bouma A. Less efficient elementary visuomotor processes in 7- to 10-year-old preterm-born children without cerebral palsy: an indication of impaired dorsal stream processes. Neuropsychology. 2008; 22:755–764. [PubMed: 18999349]

Volpe JJ. Brain injury in premature infants: a complex amalgam of destructive and developmental disturbances. Lancet Neurol. 2009; 8:110–124. [PubMed: 19081519]

Wang L, Gao Y, Shi F, Li G, Gilmore JH, Lin W, Shen D. LINKS: learning-based multi-source IntegratioN frameworK for Segmentation of infant brain images. Neuroimage. 2015; 108:160–172. [PubMed: 25541188]

Weinstein M, Marom R, Berger I, Ben Bashat D, Gross-Tsur V, Ben-Sira L, Artzi M, Uliel S, Leitner Y, Geva R. Neonatal neuropsychology: emerging relations of neonatal sensory-motor responses to white matter integrity. Neuropsychologia. 2014; 62:209–219. [PubMed: 25090927]

Westerhausen R, Huster RJ, Kreuder F, Wittling W, Schweiger E. Corticospinal tract asymmetries at the level of the internal capsule: is there an association with handedness? Neuroimage. 2007; 37:379–386. [PubMed: 17601751]

Wheeler-Kingshott CA, Cercignani M. About “axial” and “radial” diffusivities. Magn Reson Med. 2009; 61:1255–1260. [PubMed: 19253405]

Wilms M, Eickhoff SB, Specht K, Amunts K, Shah NJ, Malikovic A, Fink GR. Human V5/MT+: comparison of functional and cytoarchitectonic data. Anat Embryol (Berl). 2005; 210:485–495. [PubMed: 16328357]

Wimberger DM, Roberts TP, Barkovich AJ, Prayer LM, Moseley ME, Kucharczyk J. Identification of “premyelination” by diffusion-weighted MRI. J Comput Assist Tomogr. 1995; 19:28–33. [PubMed: 7529780]

Woods RP, Grafton ST, Holmes CJ, Cherry SR, Mazziotta JC. Automated image registration: I. General methods and intrasubject, intramodality validation. J Comput Assist Tomogr. 1998; 22:139–152. [PubMed: 9448779]

Xie S, Gong GL, Xiao JX, Ye JT, Liu HH, Gan XL, Jiang ZT, Jiang XX. Underdevelopment of optic radiation in children with amblyopia: a tractography study. Am J Ophthalmol. 2007; 143:642–646. [PubMed: 17276381]

Yamamoto A, Miki Y, Urayama S, Fushimi Y, Okada T, Hanakawa T, Fukuyama H, Togashi K. Diffusion tensor fiber tractography of the optic radiation: analysis with 6-, 12-, 40-, and 81-directional motion-probing gradients, a preliminary study. AJNR Am J Neuroradiol. 2007; 28:92–96. [PubMed: 17213432]

Yap QJ, Teh I, Fusar-Poli P, Sum MY, Kuswanto C, Sim K. Tracking cerebral white matter changes across the lifespan: insights from diffusion tensor imaging studies. J Neural Transm (Vienna). 2013; 120:1369–1395. [PubMed: 23328950]

Zhang J, Evans A, Hermoye L, Lee SK, Wakana S, Zhang W, Donohue P, Miller MI, Huang H, Wang X, van Zijl PC, Mori S. Evidence of slow maturation of the superior longitudinal fasciculus in early childhood by diffusion tensor imaging. Neuroimage. 2007; 38:239–247. [PubMed: 17826183]

Zhang L, Thomas KM, Davidson MC, Casey BJ, Heier LA, Ulug AM. MR quantitation of volume and diffusion changes in the developing brain. AJNR Am J Neuroradiol. 2005; 26:45–49. [PubMed: 15661698]

Zhang Y, Chang L, Ceritoglu C, Skranes J, Ernst T, Mori S, Miller MI, Oishi K. A Bayesian approach to the creation of a study-customized neonatal brain atlas. Neuroimage. 2014; 101:256–267. [PubMed: 25026155]

Highlights

- White matter pathways with known associated functions were mapped on the neonatal atlas.
- A cytoarchitectonic map and dynamic programing were used for the mapping.
- Normal developmental trajectories of these pathways were characterized longitudinally.
- The corpus callosum and the visual-related pathways were affected in preterm-born babies.
- Effect of preterm-birth in these pathways tends to recover during development.

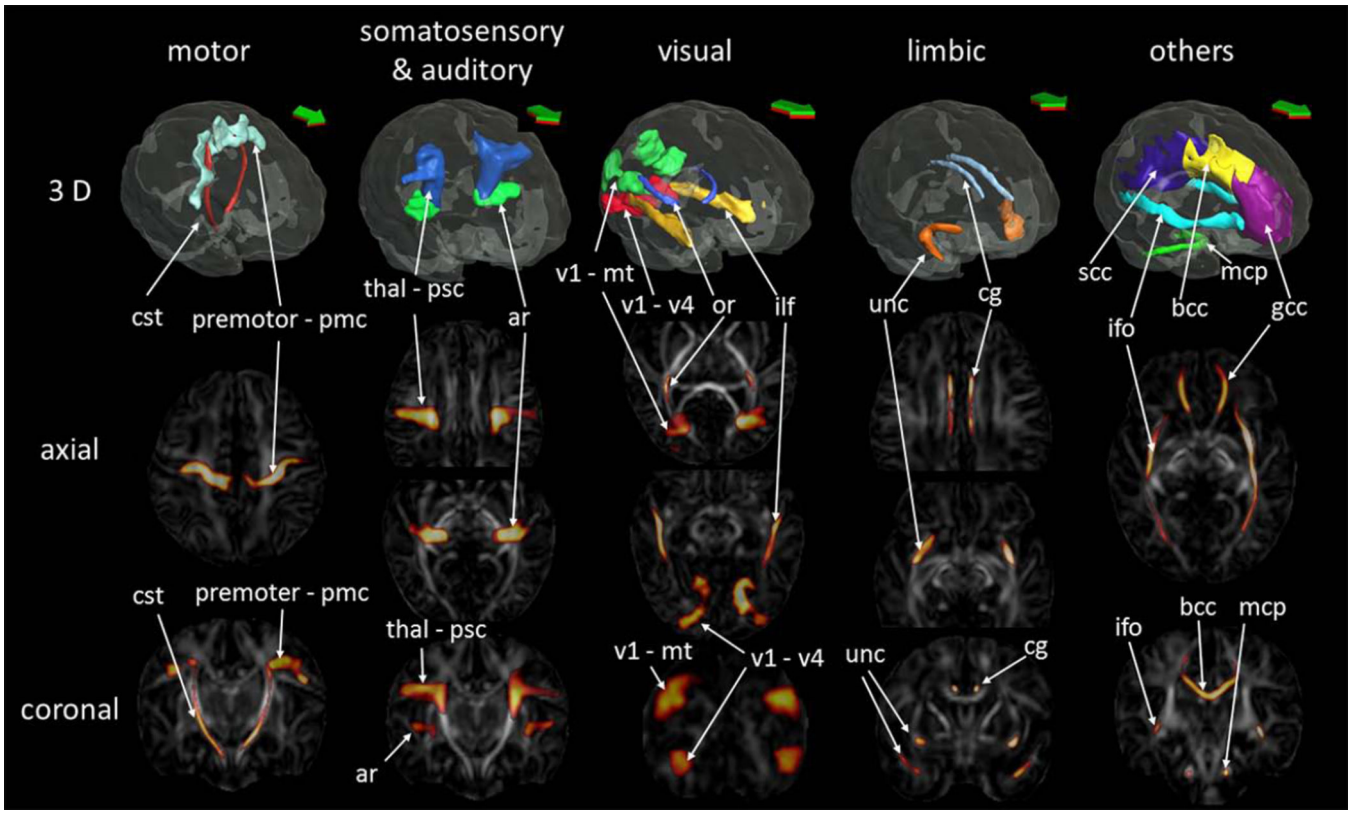

Figure 1.

Probabilistic maps of the white matter tracts with known associated functions, as well as other major white matter tracts, overlaid on the fractional anisotropy map of the JHU-neonate atlas. The three-dimensional (3D) surface of the fibers, determined by the 75% probability, was also visualized with the brain surface of the JHU-neonate-SS template (top row). AR = the acoustic radiation; BCC = the body of the corpus callosum, CG = the cingulum; CST = the corticospinal tract; GCC = the genu of the CC; IFO = the inferior fronto-occipital fasciculus; ILF = the inferior longitudinal fasciculus; MCP = the middle cerebellar peduncle; OR = the optic radiation; PMC = the primary motor cortex, PSC = the primary somatosensory cortex, SCC = the splenium of the CC, Thal = the thalamus, UNC = the uncinate fasciculus. V1-V4 = the pathway that connects the V1/V2 and the V4, V1-mt = the pathway that connects the V1/V2 and the V5/MT+.

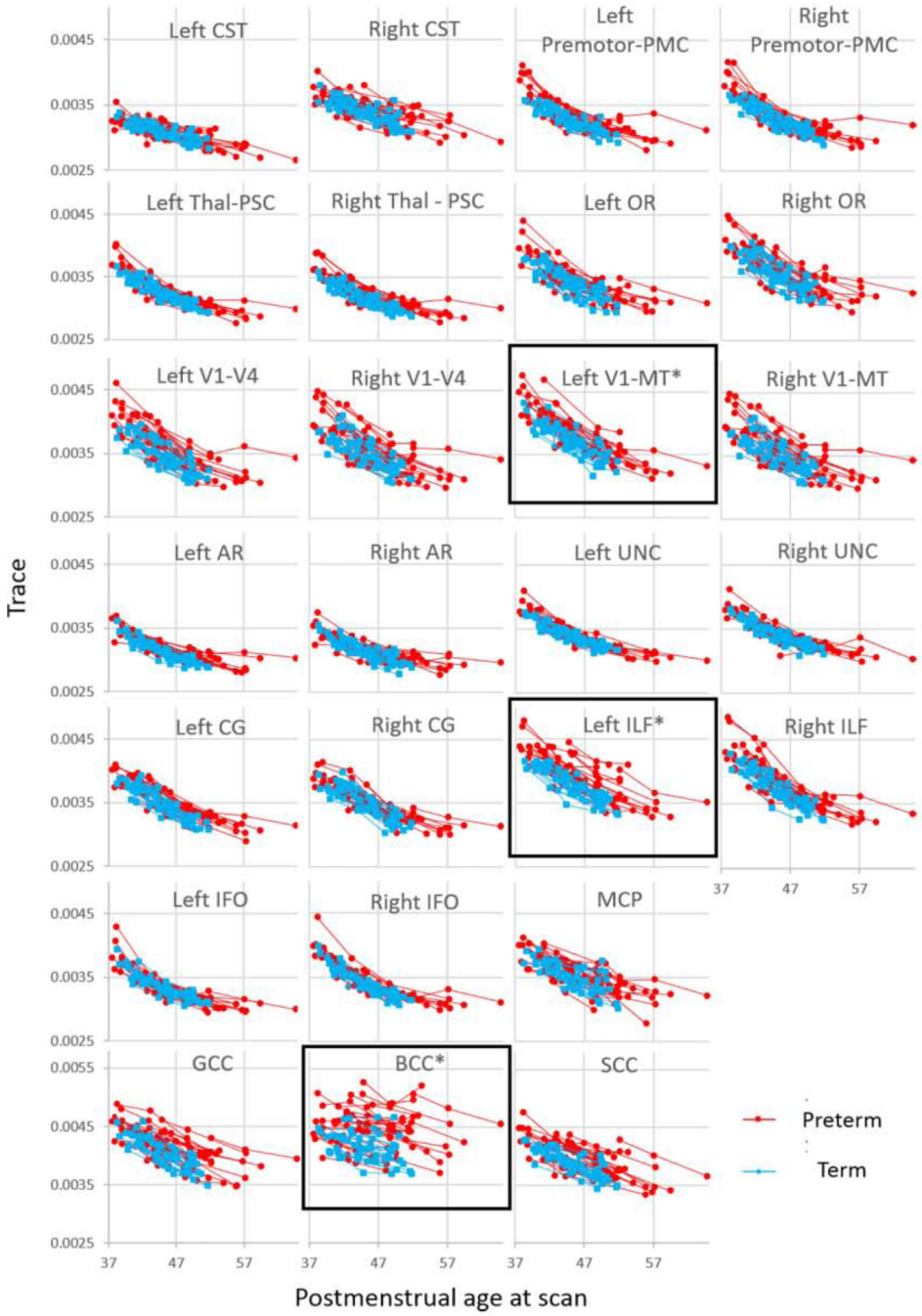

Figure 2.

Trace values of the white matter pathways. The three time points in each subject are connected with a solid line. Significant differences between term (cyan) and preterm (red) babies were identified in the body of the corpus callosum (BCC), the left inferior longitudinal fascicule (ILF), and the pathway that connects the V1/V2 and the V5/MT+ (V1-MT) and that are marked with an * and a black rectangle. AR = the acoustic radiation, CG = the cingulum, CST = the corticospinal tract, GCC = genu of the CC, IFO = the inferior fronto-occipital fasciculus, MCP = the middle cerebellar peduncle, OR = the optic radiation,

PMC = the primary motor cortex, PSC = the primary somatosensory cortex, SCC = the splenium of the CC, Thal = the thalamus, UNC = the uncinate fasciculus. V1-V4 = the pathway that connects the V1/V2 and the V4.

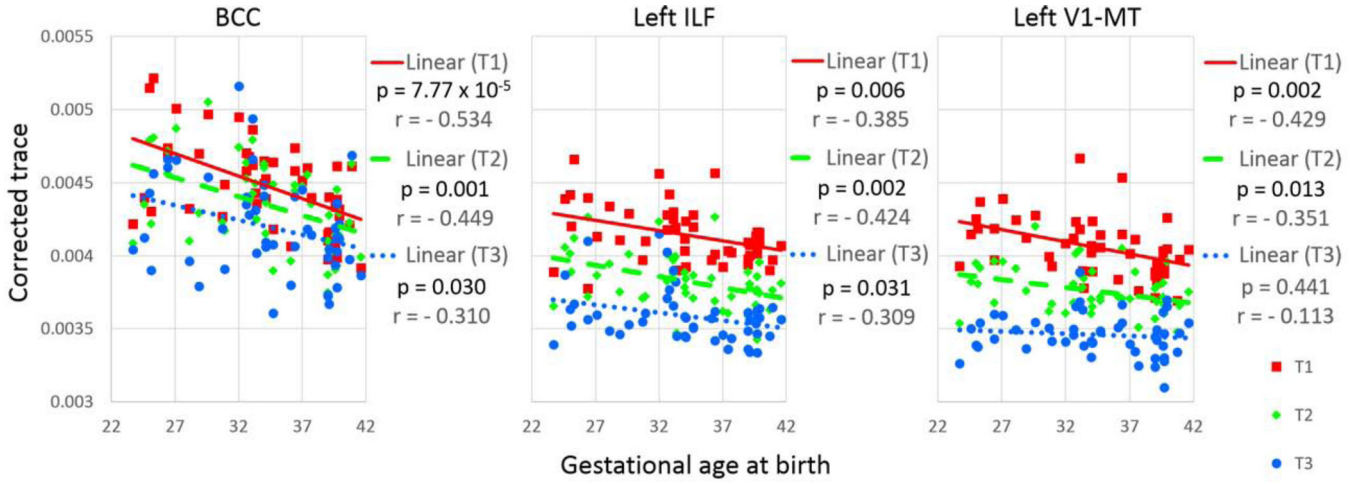

Figure 3.

Corrected trace value of each time point, plotted against gestational age at birth. BCC = the body of the corpus callosum, ILF = the inferior longitudinal fasciculus, T1 = time point 1, T2 = time point 2, T3 = time point 3. V1-MT = the pathway that connects the V1/V2 and the V5/MT+.

Table 1

Names of the neuronal pathways constructed in this study.

		Pathway Name	1st ROI	2nd ROI
Motor		CST	Cerebral peduncle	Precentral gyrus
		Premotor-PMC	Primary motor cortex	Premotor cortex (Area 6)
Sensory	Somatosensory	Thal-PSC	Sensory thalamus	Primary somatosensory cortex
	Visual	OR	Occipital lobe	Lateral geniculate body
		V1-V4	V4	V1/V2
		V1-MT	V5/MT+	V1/V2
		ILF	Hemisphere at the level of the posterior edge of the CG	Temporal lobe
	Auditory	AR	Medial geniculate body	Primary auditory cortex
Limbic		UNC	Temporal lobe	Inferior part of the frontal lobe
		CG	CG at the level of the splenium of the CC	CG at the level of the genu of the CC
Others		IFO	Occipital lobe	Frontal lobe
		MCP	MCP on one side	MCP on the other side
		CC	CC at the midsagittal plane	

AR = the acoustic radiation, CC = the corpus callosum, CG = the cingulum, CST = the corticospinal tract, IFO = the inferior fronto-occipital fasciculus, ILF = the inferior longitudinal fasciculus, MCP = the middle cerebellar peduncle, OR = the optic radiation, PMC = the primary motor cortex, PSC = the primary somatosensory cortex, thal = the thalamus, UNC; = the uncinate fasciculus, V1 = the primary visual area, V2 = the secondary visual area, V1-V4 = the pathway that connects the V1/V2 and the V4, V1-MT = the pathway that connects the V1/V2 and the V5/MT+

Table 2

Clinical characteristics of the infants.

	Full-Term (n=19)	Pre-Term (n=30)	p-value
Characteristics of infants at birth			
Gestational age {weeks; mean (range)}	39.38 (37.0 – 41.6)	30.97 (23.7 – 36.4)	**<0.0001**
Sex: Female (%) / Male (%)	9 (47.4) / 10 (52.6)	14 (46.7) / 16 (53.3)	0.9617
Race: Asian / >1 race/NHOPI[a]/White/Black/AI or AN[b]	1/15/2/0/1/0	3/17/3/6/1/0	0.2759
Ethnicity: Hispanic (%) / Non Hispanic (%)	9 (47.4) / 10 (52.6)	2 (6.7) / 28 (93.3)	**0.001**
Delivery method: C-Section (%) / Vaginal delivery (%)	3 (15.8) / 16 (84.2)	16 (53.3)/ 14 (46.7)	**0.0197**
Birth weight (kg)	3.19 ± 0.13	1.62 ± 0.12	**<0.0001**
Birth length (cm)	50.83 ± 0.81	40.90 ± 1.15	**<0.0001**
Body Mass Index (BMI) at birth	12.30 ± 0.27	9.09 ± 0.28	**<0.0001**
Birth head circumference (cm)	33.83 ± 0.31	28.49 ± 0.67	**<0.0001**
APGAR score (1 minute)	7.61 ± 0.34	6.43 ± 0.39	**0.042**
APGAR score (5 minutes)	8.82 ± 0.10	8.10 ± 0.17	**0.0049**
Retinopathy of prematurity: Yes (%) / No (%)	0 (0) / 19 (100)	8 (26.7) / 22 (73.3)	**0.0139**
Newborn audio test			0.3301
Normal (%) / Abnormal (%)	18 (94.7) / 0 (0)	29 (96.7) / 1 (3.3)	
Not reported (%)	1 (5.3)	0 (0)	
Characteristics of infants at time point 1			
Postmenstrual age {weeks; mean, (range)}	41.17 (38.3 – 44.2)	41.94 (37.6 – 52.1)	0.2725
Weight (kg)	3.51 ± 0.12	3.79 ± 0.14	0.1822
Length (cm)	51.60 ± 0.67	51.41 ± 0.74	0.8569
Head circumference (cm)	35.13 ± 0.39	35.79 ± 0.37	0.2409
Amiel-Tison Neurological Assessment (at baseline visit)			
Neurosensory function	0.39 ± 0.14	0.40 ± 0.16	0.9618
Passive muscle tone	0.06 ± 0.06	0.07 ± 0.05	0.881
Active muscle tone	5.33 ± 0.41	4.43 ± 0.37	0.1231
Primitive reflexes	0.06 ± 0.06	0.10 ± 0.06	0.5989
Deep tendon reflexes	0 ± 0	0 ± 0	NA
Cranial assessment	0 ± 0	0 ± 0	NA
Adaptiveness to manipulation	0 ± 0	0.17 ± 0.07	0.0697
Total neurological examination score	5.83 ± 0.39	5.17 ± 0.51	0.3627
Age of infants based on postmenstrual weeks at follow-up MRI scan {weeks; mean, (range)}			
Time point 2	45.06 (42.0 – 46.9)	46.62 (41.8 – 57.1)	**0.0307**
Time point 3	49.36 (47.1 – 51.8)	51.74 (42.7 – 64.7)	**0.0095**
Characteristics of the Parent or Primary Caregiver			

	Full-Term (n=19)	Pre-Term (n=30)	p-value
Mother's age at time of infant's birth (years)	26.68 ± 1.56	31.87 ± 0.80	**0.0021**
Mother's pregnancy weight gain (kg)	19.32 ± 2.47	13.92 ± 1.69	0.0673
Mother's head circumference (cm)	57.86 ± 0.59	56.84 ± 0.47	0.1835
Mother's education (years)	12.90 ± 0.60	14.87 ± 0.47	**0.0125**
Socioeconomic status (index of social position)	56.47 ± 3.18	34.93 ± 2.42	**<0.0001**
Edinburgh postnatal depression scale (baseline visit)	7.53 ± 1.36	6.00 ± 0.99	0.3607

[a] NHOPI (Native Hawaii and Other Pacific Islanders)

[b] AI or AN (American Indian or Alaskan Natives)

Table 3

Differences in the trace values between the left and the right side of the pathways. The results are sorted by the hemisphere effect from lower to higher p value. A: term-born babies, B: preterm-born babies; CST = the corticospinal tract; IFO = the inferior fronto-occipital fasciculus; OR = the optic radiation; PSC = the primary somatosensory cortex; Thal = the thalamus.

A

	Hemisphere effect (p)	**Pairwise comparison (p)**		
		Time Point 1	**Time Point 2**	**Time Point 3**
CST	7.41×10^{-14}	8.92×10^{-18}	7.49×10^{-16}	7.32×10^{-15}
OR	0.004	4.20×10^{-5}	0.001	0.005
Thal-PSC	0.008	0.001	0.001	0.018

B

	Hemisphere effect (p)	Pairwise comparison (p)		
		Time Point 1	Time Point 2	Time Point 3
CST	6.75×10^{-18}	1.11×10^{-21}	4.77×10^{-18}	1.88×10^{-18}
IFO	0.002	0.001	0.005	0.030
OR	0.011	0.001	0.003	0.019

Table 4

Corrected trace values of each time point and the difference between term- and preterm-born groups. Results are sorted by the group effect from lower to higher p value.

		Corrected trace; mean (range)			Group effect (p)	Pairwise comparison (p)		
		Time Point 1	Time Point 2	Time Point 3		Time Point 1	Time Point 2	Time Point 3
BCC	term	0.00428 (0.00391–0.00461)	0.00421 (0.00374–0.00462)	0.00410 (0.00374–0.00469)	0.009	1.90×10^{-4}	3.05×10^{-4}	2.88×10^{-3}
	preterm	0.00460 (0.00407–0.00522)	0.00445 (0.00389–0.00505)	0.00427 (0.00358–0.00515)				
Lt.ILF	term	0.00403 (0.00389–0.00415)	0.00372 (0.00342–0.00395)	0.00353 (0.00333–0.00373)	0.010	2.26×10^{-3}	6.55×10^{-4}	1.33×10^{-3}
	preterm	0.00419 (0.00371–0.00463)	0.00388 (0.00346–0.00428)	0.00362 (0.00339–0.00415)				
Lt.V1-MT	term	0.00393 (0.00365–0.00431)	0.00367 (0.00345–0.00402)	0.00340 (0.00307–0.00373)	0.031	3.82×10^{-4}	1.34×10^{-2}	1.30×10^{-2}
	preterm	0.00413 (0.00374–0.00472)	0.00379 (0.00355–0.00422)	0.00347 (0.00326–0.00387)				
Rt.ILF	term	0.00401 (0.00384–0.00418)	0.00367 (0.00336–0.00384)	0.00341 (0.00319–0.00355)	0.084			
	preterm	0.00411 (0.00372–0.00461)	0.00381 (0.00344–0.00431)	0.00351 (0.00331–0.00375)				
GCC	term	0.00428 (0.00405–0.00459)	0.00398 (0.00370–0.00427)	0.00378 (0.00347–0.00404)	0.088			
	preterm	0.00441 (0.00401–0.00480)	0.00416 (0.00365–0.00471)	0.00388 (0.00351–0.00428)				
Lt.V1-V4	term	0.00369 (0.00342–0.00397)	0.00342 (0.00320–0.00371)	0.00319 (0.00301–0.00349)	0.114			
	preterm	0.00388 (0.00351–0.00441)	0.00357 (0.00314–0.00400)	0.00328 (0.00302–0.00361)				
SCC	term	0.00408 (0.00382–0.00423)	0.00387 (0.00357–0.00407)	0.00364 (0.00341–0.00400)	0.158			
	preterm	0.00423 (0.00391–0.00469)	0.00398 (0.00360–0.00428)	0.00373 (0.00340–0.00411)				
Rt.Thal-PSC	term	0.00336 (0.00320–0.00353)	0.00313 (0.00302–0.00325)	0.00299 (0.00286–0.00308)	0.170			
	preterm	0.00344 (0.00320–0.00372)	0.00321 (0.00299–0.00345)	0.00302 (0.00284–0.00317)				
Lt.CG	term	0.00369 (0.00348–0.00394)	0.00343 (0.00322–0.00368)	0.00317 (0.00306–0.00341)	0.305			
	preterm	0.00375 (0.00349–0.00398)	0.00351 (0.00327–0.00376)	0.00324 (0.00301–0.00341)				
Lt.Premotor-PMC	term	0.00345 (0.00327–0.00355)	0.00322 (0.00309–0.00336)	0.00309 (0.00292–0.00330)	0.381			
	preterm	0.00356 (0.00328–0.00392)	0.00330 (0.00305–0.00360)	0.00313 (0.00289–0.00333)				

		Corrected trace; mean (range)			Group effect (p)	Pairwise comparison (p)		
		Time Point 1	Time Point 2	Time Point 3		Time Point 1	Time Point 2	Time Point 3
Rt.IFO	term	0.00361 (0.00342–0.00379)	0.00336 (0.00324–0.00344)	0.00318 (0.00306–0.00328)	0.610			
	preterm	0.00369 (0.00345–0.00420)	0.00341 (0.00325–0.00371)	0.00321 (0.00307–0.00337)				
Rt.UNC	term	0.00358 (0.00345–0.00371)	0.00338 (0.00323–0.00348)	0.00320 (0.00304–0.00331)	0.857			
	preterm	0.00363 (0.00329–0.00393)	0.00342 (0.00325–0.00366)	0.00323 (0.00311–0.00331)				
Lt.AR	term	0.00330 (0.00314–0.00347)	0.00309 (0.00294–0.00323)	0.00296 (0.00284–0.00307)	0.893			
	preterm	0.00334 (0.00311–0.00356)	0.00314 (0.00300–0.00332)	0.00299 (0.00286–0.00316)				
Rt.Premotor-PMC	term	0.00348 (0.00325–0.00361)	0.00322 (0.00308–0.00343)	0.00308 (0.00290–0.00321)	0.917			
	preterm	0.00357 (0.00335–0.00398)	0.00330 (0.00310–0.00363)	0.00311 (0.00293–0.00340)				
Lt.UNC	term	0.00356 (0.00341–0.00365)	0.00335 (0.00325–0.00345)	0.00319 (0.00308–0.00329)	0.933			
	preterm	0.00362 (0.00340–0.00392)	0.00339 (0.00324–0.00354)	0.00321 (0.00310–0.00329)				
Lt.OR	term	0.00364 (0.00337–0.00382)	0.00334 (0.00310–0.00356)	0.00315 (0.00294–0.00339)	1.000			
	preterm	0.00371 (0.00340–0.00422)	0.00343 (0.00314–0.00380)	0.00322 (0.00302–0.00347)				
Rt.V1-V4	term	0.00377 (0.00340–0.00412)	0.00348 (0.00329–0.00373)	0.00325 (0.00303–0.00349)	1.000			
	preterm	0.00389 (0.00344–0.00433)	0.00357 (0.00316–0.00403)	0.00332 (0.00304–0.00378)				
Rt.AR	term	0.00329 (0.00314–0.00344)	0.00311 (0.00292–0.00327)	0.00297 (0.00278–0.00316)	1.000			
	preterm	0.00331 (0.00309–0.00360)	0.00315 (0.00295–0.00333)	0.00302 (0.00282–0.00315)				
Lt.Thal-PSC	term	0.00344 (0.00330–0.00358)	0.00320 (0.00307–0.00334)	0.00303 (0.00294–0.00312)	1.000			
	preterm	0.00349 (0.00325–0.00383)	0.00325 (0.00304–0.00350)	0.00305 (0.00285–0.00325)				
Rt.CST	term	0.00353 (0.00340–0.00373)	0.00337 (0.00320–0.00354)	0.00322 (0.00307–0.00355)	1.000			
	preterm	0.00359 (0.00331–0.00394)	0.00341 (0.00312–0.00371)	0.00328 (0.00302–0.00353)				
Rt.OR	term	0.00383 (0.00351–0.00405)	0.00348 (0.00321–0.00370)	0.00328 (0.00309–0.00352)	1.000			
	preterm	0.00387 (0.00343–0.00430)	0.00357 (0.00321–0.00398)	0.00333 (0.00302–0.00370)				

		Corrected trace; mean (range)			Group effect (p)	Pairwise comparison (p)		
		Time Point 1	Time Point 2	Time Point 3		Time Point 1	Time Point 2	Time Point 3
MCP	term	0.00371 (0.00354–0.00389)	0.00346 (0.00327–0.00369)	0.00330 (0.00304–0.00374)	1.000			
	preterm	0.00377 (0.00348–0.00402)	0.00355 (0.00323–0.00380)	0.00332 (0.00286–0.00359)				
Rt.CG	term	0.00373 (0.00351–0.00400)	0.00347 (0.00330–0.00368)	0.00320 (0.00299–0.00342)	1.000			
	preterm	0.00375 (0.00350–0.00403)	0.00351 (0.00336–0.00389)	0.00323 (0.00302–0.00338)				
Rt.V1-MT	term	0.00392 (0.00367–0.00417)	0.00362 (0.00337–0.00386)	0.00339 (0.00312–0.00369)	1.000			
	preterm	0.00402 (0.00362–0.00438)	0.00366 (0.00326–0.00406)	0.00341 (0.00307–0.00403)				
Lt.IFO	term	0.00353 (0.00332–0.00374)	0.00329 (0.00313–0.00342)	0.00314 (0.00300–0.00328)	1.000			
	preterm	0.00357 (0.00334–0.00408)	0.00331 (0.00317–0.00349)	0.00313 (0.00296–0.00325)				
Lt.CST	term	0.00319 (0.00308–0.00330)	0.00306 (0.00296–0.00319)	0.00293 (0.00282–0.00311)	1.000			
	preterm	0.00321 (0.00302–0.00346)	0.00308 (0.00295–0.00319)	0.00294 (0.00276–0.00318)				

AR = the acoustic radiation, BCC = body of the corpus callosum, CG = the cingulum, CST = the corticospinal tract, GCC = the genu of the corpus callosum, IFO = the inferior fronto-occipital fasciculus, ILF = the inferior longitudinal fasciculus, Lt. = left, MCP = the middle cerebellar peduncle, OR = the optic radiation, PMC = the primary motor cortex, PSC = the primary somatosensory cortex, Rt. = right, SCC = the splenium of the corpus callosum, Thal = the thalamus, UNC = the uncinate fasciculus, V1-V4 = the pathway that connects the V1/V2 and the V4, V1-MT = the pathway that connects the V1/V2 and the V5/MT+.